Applied Energy 408 (2026) 127402

Contents lists available at ScienceDirect

Applied Energy

journal homepage: www.elsevier.com/locate/apen

Sequential operation of residential energy hubs using physics-based economic nonlinear MPC

Darío Slaifstein*, Gautham Ram Chandra Mouli, Laura Ramirez-Elizondo, Pavol Bauer

DC Systems, Energy Conversion & Storage, Electrical Sustainable Energy Department, Delft University of Technology, Mekelweg 8, Delft, 2628, Zuid-Holland, Netherlands

HIGHLIGHTS

- Physics-based EMPC optimizes building comfort, EV V2G, and battery health across diverse market and flexibility settings.
- Operating in intraday markets saves costs but accelerates battery degradation, contradicting literature day-ahead models.
- Under sequential markets, batteries and EVs provide short-term flexibility; while the thermal storage value is marginal.

GRAPHICAL ABSTRACT

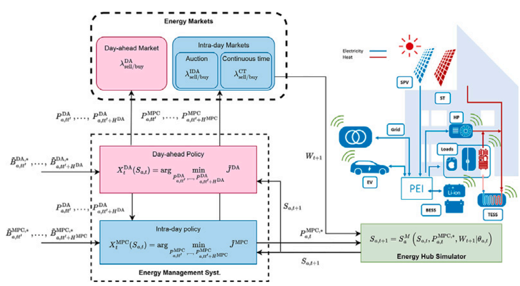

ARTICLE INFO

2000 MSC:
0000
1111

PACS:
0000
1111

Keywords:
Energy management
Sequential energy markets
Multi-carrier energy storage

ABSTRACT

The operation of residential energy hubs with multiple energy carriers (electricity, heat, mobility) poses a significant challenge due to different carrier dynamics, hybrid storage coordination and high-dimensional action-spaces. Energy management systems oversee their operation, deciding the set points of the primary control layer. This paper presents a novel 2-stage economic model predictive controller for electrified buildings including physics-based models of the battery degradation and thermal systems. The hierarchical control operates in the Dutch sequential energy markets. In particular common assumptions regarding intra-day markets (auction and continuous-time) are discussed as well as the coupling of the different storage systems. The best control policy it is best to follow continuous time intra-day in the summer and the intra-day auction in the winter. This sequential operation comes at the expense of increased battery degradation. Lastly, under our controller, the realized short-term flexibility of the thermal energy storage is marginal compared to the flexibility delivered by stationary battery pack and electric vehicles with bidirectional charging.

* Corresponding author.
Email address: d.a.slaifstein@tudelft.nl (D. Slaifstein).

https://doi.org/10.1016/j.apenergy.2026.127402
Received 29 July 2025; Received in revised form 22 December 2025; Accepted 8 January 2026
Available online 14 January 2026

Nomenclature

Optimization, Control & Dynamics

$\lambda_{\text{buy/sell},t}$ Day-ahead buy and sell prices.
$\mathbb{E}_W$ Expectation with respect to the exogenous process W.
$\mathcal{D}_t^\pi = [t; t+H]$ Prediction horizon window at time t.
$\mathcal{P}_{a,[t,t+H]}$ Power trajectory for system a over horizon $[t, t+H]$.
$\mathcal{S}_{a,[t,t+H]}$ State trajectory for system a over horizon $[t, t+H]$.
$\overline{\ }, \underline{\ }$ Maximum and minimum variable bounds.
π Policy.
$\theta_{a,t}$ Model parameters for system a at time t.
$\tilde{\ }$ Approximated/estimated variable/function.
ε_{SoC} Deviation from required departure SoC.
$^+, ^-$ Positive and negative variable components.
$a \in \mathbb{A}$ Set of energy assets.
$b \in \{\text{BESS}, \text{EV}\} \subset a$ Battery storage asset index.
$B_{a,t}$ Belief state for asset a at time t.
C_{grid} Cost of electricity from the grid.
C_{loss} Loss cost or penalty.
p_{SoCDep} Penalty for EV charging.
$P_{a,t} \in \mathcal{P}$ Power setpoint for system a at time t.
$p_{T_{\text{in}}}$ Penalty for thermal comfort.
$S_{a,t}^M(\cdot)$ Transition function for asset a at time t.
$S_{a,t} \in \mathcal{S}$ State of system a at time t.
T, H Simulation and optimization horizons.
$t, t', \Delta t$ Time index, time index within a policy π and timestep.
$w = [w_{\text{grid}}, w_{\text{loss}}, w_{\text{SoC}}, w_{\text{TESS}}]$ Objective function weights.
W_{t+1} Exogenous information process at time $t+1$.
$X_t^\pi(\cdot)$ Policy function at time t.

Battery Performance Model

η_c Coulombic efficiency.
$\tilde{S}_{b,t}^M(\cdot)$ Battery transition model with performance and ageing
$d_{b,t}^M(\cdot)$ Battery ageing model.
$N_{p,b}$ Number of parallel branches.
$N_{s,b}$ Number of cells in series.
$OCV_{b,t}$ Open-circuit voltage at time t.
$p_{b,t}^M(\cdot)$ Battery performance model.
$Q_{b,t}$ Battery capacity at time t.
$S_{b,t} = [SoC, v_t]_{b,t}^T$ Battery state vector at time t
$SoC_{b,t}$ State of Charge of battery b at time t
$t_{0,b}$ Battery elapsed lifetime
$v_{t,b,t}$ Terminal voltage of battery b
$x_{b,t} = i_{b,t}$ Control cell current to the battery model at time t

Battery Degradation Model

$\delta_{\text{SEI},b,t}$ SEI layer thickness
$\eta_{k,b,t}$ SEI kinetic overpotential
$\varepsilon_{e,b,t}$ Electrolyte volume fraction
$i_{\text{AM},b,t}$ Active material loss current
$i_{\text{SEI},b,t}$ SEI side reaction current
$i_{\text{loss},b,t}$ Total degradation current
$OCV_{n,b,t}$ Open-circuit voltage of anode
SoH State of Health of the battery
$z_{b,t}, z_{b,0\%}, z_{b,100\%}$ Lithium stoichiometry at time t, and limits at 0 and 100%

Electric Vehicle (EV) Model

$\gamma_{\text{EV},t}$ EV availability at time t (1 = parked, 0 = driving)
$P_{\text{EV},t}$ EV charger power at time t
$P_{\text{tot,EV},t}$ Total power associated with EV at time t
$P_{\text{drive,EV}}$ Power consumed while driving
SoC_{dep}^* Required SoC at departure
$t_{\text{dep/arr}} \sim \mathcal{T}_{\text{dep/arr}}$ Departure and arrival time of the EV

Thermal Models

$\dot{Q}_t$ Heat transfer rate (e.g., $\dot{Q}_{\text{ir},t}$, $\dot{Q}_{\text{loss},t}$, $\dot{Q}_{\text{cond},t}$, $\dot{Q}_{\text{vent},t}$, $\dot{Q}_{\text{sd},t}$, $\dot{Q}_{\text{cond}}$)
COP_t Coefficient of performance of the heat pump at time t
$G_{\text{ir},t}$ Incident solar irradiance at time t
$s_{T_{\text{in}}}$ Building temperature slack variable
T_t Temperature (e.g., $T_{\text{in},t}$, $T_{\text{amb},t}$, $T_{\text{TESS},t}$, $T_{\text{HP},t}$).

1. Introduction

In the context of the energy transition, building electrification poses a significant techno-economic challenge. It is in buildings where different electrification processes intersect most tangibly, with the incorporation of private electric vehicles (EVs) and the replacement of traditional gas-boilers with heat-pumps [1,2]. Harnessing synergies between the different carriers can contribute to more sustainable, flexible, and cost-efficient energy solutions at various levels of the system [3–10]. To capitalize on such opportunities, system integration and control strategies must be purposefully designed in the multicarrier energy systems (MCES). This integration relies on advanced energy management systems (EMS) capable of coordinating and optimizing the operation of multi-carrier energy storage systems. These must operate within dynamic and uncertain environments in a consistent and reliable manner [11,12]. Moreover, in the future, the participation of these new buildings in energy and power markets appears to be an attractive economic opportunity [12–14].

2. Literature review

Currently, various sequential electricity markets are implemented across Europe and the US. The day-ahead (DA) market is cleared one day before operation at D-1. Bids are composed of 24hr, 1hr timestep, production and demand schedules. After that, different intra-day markets are opened one or more times (depending on the country) before day D to adjust schedules to recent forecasts. These include pay-as-clear intra-day auctions (IDA) a couple of hours before the time of delivery and a continuous-time intra-day (CT) market at delivery time with a pay-as-bid mechanism. In auctions, block bids may have different sizes (1-4hrs) and time resolutions (5-15min) depending on the country. The continuous-time intra-day market is organized in an order-book which stays open for a day until the time of delivery. Usually, these markets are opened by the transmission system operator (TSO) and/or independent system operator (ISO). On a smaller time scale, different balancing markets are offered by the TSO and distribution system operators (DSOs). Traditionally, frequency markets are related to TSOs at the high voltage (HV) level, whereas novel local imbalance/congestion markets are being implemented by DSOs at the MV/LV level. In this paper, the focus is on the day-ahead auction (DA), the intra-day auctions (IDA), and intra-day continuous time (CT).

Several studies have proposed operating MCES in energy markets [12–16]. Currently, there are limited options to dispatch and operate residential energy hubs/electrified buildings in the EU or US energy markets due to their current minimum power and energy requirements. Moreover, traditional economic models (marginal costs) have limited capabilities to describe distributed energy resources (DER) operation in sequential electricity markets. The reader may remember that traditional liberalized energy markets assume non-strategic bidding from their market participants [17]. However, it is worth studying the integration of MCES in sequential energy markets to inform future market designs and stakeholders.

The main references for this work are presented in Table 1. The literature presents several works dealing with MCES in sequential

Table 1
Summary of literature review.

Ref.	Application	Loads / carriers			Flexibility					Markets		Policy type
		Elec. load	Space heating	Nat.gas	TESS	EV	BESS	Heat pump	Battery ageing	Day-ahead	Intra-day	
[7,8,18]	Multi-Energy Sys.(2MW)	✓	✓	✓	✓		✓	✓		✓		Safety focused RL
[19]	Building	✓	✓				✓			✓		RL-DDPG
[20]	Buildings	✓	✓	✓		✓				✓		MARL
[21]	Building	✓	✓				✓			✓		Safe-MDRL
[22]	Industry (4MW)	✓					✓			✓		SC-RL
[23]	Industry (70MW)	✓	✓	✓			✓			✓		PLSAC-RL
[12]	Multi-Energy (2MW)	✓	✓	✓			✓			✓	Scaled prices	2-stage eMPC
[14]	Multi-Energy (1MW)	✓	✓	✓	✓		✓	✓		✓	Scaled prices	3-stage hier. MPC
[24]	Building	✓	✓	✓	✓		✓			✓	No trading	Schedule & eMPC
[13]	Microgrid aggregation	✓		H2	H2		✓		Empirical	✓	Scaled prices	3-stage eMPC
This work	Small Building	✓	✓		✓	✓	✓	✓	✓	✓	✓	2-stage eMPC

markets and ancillary services [12–16]. For day-ahead schedules, Zhou [15] uses a robust approach to schedule the bids of energy communities in both energy and frequency DA markets. Similarly, Vermeer [25] presents a deterministic DA and FCR for a building with a battery energy storage system (BESS) and EV, without controlling the thermal carrier. Li et al. [14] presents a hierarchical optimization to control an industrial MCES with power, heat, cooling and gas in 3 different timescales (1hr, 15min and 5min) to capture carrier dynamics, but doesn't include the mobility carrier. Unfortunately, their approach is based only on marginal costs, with no ties to dynamic market prices, and only presents first-order dynamics. References [7,8,18–23], use reinforcement learning techniques to substitute model-based approaches, but the agents only operate in the DA market and do not always include flexible heating systems nor smart EV charging. Recently, Jouini [12] presented a sequential EMS for MCES operating in DA and intra-day energy markets, where the intra-day layer used economic MPC (eMPC) [26]. Besides Jouini [12] the most complete work is by Gros [24]. It presents a CHP based microgrid and a 2-stage Model Predictive Control (MPC) to control it. Unfortunately, the heating is not electrified, and it is not integrated into intra-day markets. All references that take into account intra-day markets refer only to the continuous-time (CT) intra-day market, assuming that this market follows the same dynamics as the day-ahead market and only scales the day-ahead prices. This assumption disregards the different frequency components and volatility of the DA, IDA and CT leading to a poor dynamic analysis of the storage systems used. Finally, only 1 (one) work accounts for EV integration [20] but disregards numerous other aspects (intra-day market, hybrid energy storage system (HESS), battery ageing, etc.). The interaction between the different storage systems (BESS, EV, and thermal energy storage system (TESS)) depends on the various price signals being followed. Hence, how these elements interact is crucial to understanding multi-carrier systems.

Regarding the current white-box or MPC policy approaches, their dynamic models are limited to simplified linear time-invariant systems. Moreover, most works only focus on one carrier at a time [5,25,27,28]. To coordinate HESS, the different technologies must be modeled, representing power limits, dynamics, and other particularities. Heating models focusing on thermal comfort are based on building and device thermodynamics [28–31]. A TESS will have different dynamics depending on its technology and a heat pump (HP) will present nonlinear conversion efficiencies if they are air-air, air-water, and so on [30,31]. To model the heating approximating it as a flow can be an option. Nevertheless, it assumes a fixed temperature setpoint, reducing operational flexibility and hindering the tractability of the underlying optimal control problem [8,12,14,23].

Another critical modelling point is battery degradation, as its operation affects the lifetime; thus, ambitious controls might hinder it. Detailed battery models are usually reserved for local controls, whereas EMS formulations for residential MCES tend to simplify the models to linear or quadratic forms, overlooking most technological particularities like chemistry, diffusion dynamics, or capacity fade [4,7,10,29,32]. Implementing approximated empirical models that are not meant for control applications is the standard practice [33]. Unfortunately, such degradation models only have interpolation capabilities, typically use non-linear equations, represent a limited number of operating conditions (average C-rate, minimum SoC, etc.), are prone to overfitting, and are chemistry dependent. On the other hand, physics-based (PB) models are built through first-principles and specialized tests to identify individual degradation mechanisms [34–37]. They have extrapolation features, can be expressed in the state-space form, account for several cathode chemistries, and represent a wide range of operating conditions. Even though they are non-linear and non-convex, they have been integrated into different optimal control schemes through control-oriented physics-based reduced order model (PBROM) and demonstrating greater potential cost savings than their empirical counterparts [27,33–36,38–45]. Overlooking these modelling assumptions (battery degradation and thermal controls) hinders the accuracy, generality, and practicality of the results in the literature, since potential interactions between systems are limited by them.

Summing up, five main gaps can be identified in the literature:

1. Usually, intra-day markets are only addressed by scaling the prices of the DA market. This simplification does not consider the differences between intra-day auctions and continuous time intra-day, especially in their frequency spectrum, leading to sub-optimal decisions [46,47]. Is it still true for integrated energy systems? How does it impact battery degradation?
2. Integration of electrified buildings with integrated mobility in sequential markets has been introduced, but it has not included bidirectional charging, nor its stochastic availability. Improving these aspects presents an opportunity for additional flexibility and added value.
3. Joint operation of hybrid energy storage systems that combine BESS, TESS, and EV is uncommon. Integrated operation could unlock synergies between carriers and storage systems. In other words, do individual energy storage systems (ESS) performances prevail, or is there a limitation in their interaction?
4. Battery degradation has been studied using empirical models that were not meant for dynamic operation and integration in EMS schemes. This leads to suboptimal results and reduced flexibility [33]. For example, preventing battery degradation through solid electrolyte interface (SEI) control incentivizes the battery to be discharged $SoC \rightarrow \underline{SoC}$ [37,40,45]. Does this affect the rest of the HESS? Is this still valid under higher frequency prices? Can degradation be controlled without sacrificing grid benefits [42]?
5. Detailed thermal modelling is often reserved for studies where single-carrier systems are analyzed. Accounting for nonlinear HP behavior and utilizing a comfort band to control temperature unlocks potential savings and flexibilities that actively interact with HESS components.

To address such gaps the contributions of this paper are:

1. A novel two-level economic model predictive control EMS for residential energy hubs that integrates: day-ahead and intra-day markets, PBROM ageing models for battery-based ESS, flexible electrical heating control, and EV bidirectional smart-charging.
2. An in-depth analysis of the residential energy hub participation in the day-ahead and intra-day markets using real data from [48].
3. A detailed analysis of the interaction between electric and thermal carriers, including BESS, EV, and TESS, in the context of electrified buildings under deterministic and noisy settings.
4. An open-source library for implementing optimization-based EMS for multiple applications.

A schematic of the system under study is presented in Fig. 1. The building is composed of solar photovoltaics (SPV), a battery energy storage system (BESS), an electric vehicle (EV), a power electronic interface (PEI), a heat pump (HP), a thermal energy storage system (TESS), a grid connection, and loads. This paper focuses on optimizing the flows behind this grid connection for a single system, with the aim of showing the potential behind such applications. Each level of the EMS corresponds to an energy market. The first layer consists of a planner participating in the day-ahead market, and the second layer is an eMPC participating in the intra-day markets.

This manuscript is organized as follows: section 3 presents the problem and modelling framework, section 4 presents the algorithm design and models used; section 5 describes our case studies and validation; finally section 6 presents the conclusions and future works.

3. Sequential market models

The following section describes the EMS models, following the Universal Modelling Framework (UMF) by Powell [49,50] and the models developed in [45]. For a given system size, the objective is to handle the operational cost, which is composed of four parts: the net cost of energy from the grid C_{grid}, the degradation cost of losing storage capacity C_{loss}, a penalty for not charging the EV at departure p_{SoCDep} and a penalty to ensure thermal comfort p_T. The grid cost, the degradation cost and the thermal discomfort are cumulative objectives because the goal is to optimize them through time, while the penalty for not charging the EV to the desired SoC is only a point penalty at departure times t_{dep}. The sequential decision problem (SDP) is then:

$$\min_{x^*_{a,t}} \quad \mathbb{E}_W[C_{\text{grid}} + C_{\text{loss}} + p_{\text{SoCDep}} + p_T] \tag{1a}$$

$$\text{s.t.} \quad S_{a,t+1} = S^M_{a,t}(S_{a,t}, x^*_{a,t}, W_{t+1}|\theta_{a,t}) \tag{1b}$$

$$x^*_{a,t} = X^\pi_t(S_{a,t}) \in \mathcal{X} \qquad \forall a \in \mathbb{A},\ t \in \mathcal{D}_t \tag{1c}$$

$$S_{a,t} \in \mathcal{S} \qquad \forall a \in \mathbb{A},\ t \in \mathcal{D}_t \tag{1d}$$

$$\mathbb{A} = \{\text{SPV}, \text{grid}, \text{EV}, \text{BESS}, \text{HP}, \text{TESS}\} \tag{1e}$$

where $S_{a,t}$ is the state vector, $x^*_{a,t}$ is the optimal decision for timestep t, W_{t+1} is an exogenous process that introduces new information after making a decision. The mappings $S^M_{a,t}(\cdot)$, and $X^\pi_t(\cdot)$ are the transition function and optimal policy, respectively. The first is a set of equations describing the states and parameter evolution, and the second is the algorithm that finds the setpoints. The vector $\theta_{a,t}$ contains all the parameters of each asset a and changes over time t. The subindex $a \in \mathbb{A}$ corresponds to the assets shown in Fig. 1. The index $b \in \{\text{BESS}, \text{EV}\} \subset a$ denotes the electric storage assets. The simulation time is T and the timestep is Δt and the time domain is $\mathcal{D}_t = [0, \Delta t, \dots, T]$.

The components of the objective are presented in Fig. 2. From top to bottom the first component is grid cost C_{grid} defined by the cost in each market:

$$C_{\text{grid}} = C^{\text{DA}}_{\text{grid}} + C^{\text{MPC}}_{\text{grid}} \tag{2a}$$

$$C^{\text{DA/MPC}}_{\text{grid}} = w_{\text{grid}} \sum_{t=0}^{T} c^{\text{DA/MPC}}_{\text{grid},t}.\Delta t \tag{2b}$$

$$c^{\text{DA}}_{\text{grid},t} = \frac{\lambda^{\text{DA}}_{\text{buy},t} - \lambda^{\text{DA}}_{\text{sell},t}}{2} |P^{\text{DA}}_{\text{grid},t}| + \frac{\lambda^{\text{DA}}_{\text{buy},t} + \lambda^{\text{DA}}_{\text{sell},t}}{2} P^{\text{DA}}_{\text{grid},t} \tag{2c}$$

$$c^{\text{MPC}}_{\text{grid},t} = \frac{\lambda^{\text{MPC}}_{\text{buy},t} - \lambda^{\text{MPC}}_{\text{sell},t}}{2} \left|\Delta P_{\text{grid},t}\right| + \frac{\lambda^{\text{MPC}}_{\text{buy},t} + \lambda^{\text{MPC}}_{\text{sell},t}}{2} \Delta P_{\text{grid},t} \tag{2d}$$

$$\Delta P_{\text{grid},t} = P^{\text{MPC}}_{\text{grid},t} - P^{\text{DA}}_{\text{grid},t} \tag{2e}$$

The superscripts DA and MPC denote the layer of the controller, with the MPC layer connected to an intra-day market. The subscripts "buy" and "sell" denote each price, w_{grid} is a user-defined weight, λ_t are the market prices, and $P_{\text{grid},t}$ is the grid power. The formulation from [12,13] is chosen due to its robustness and numerical properties. In this work,

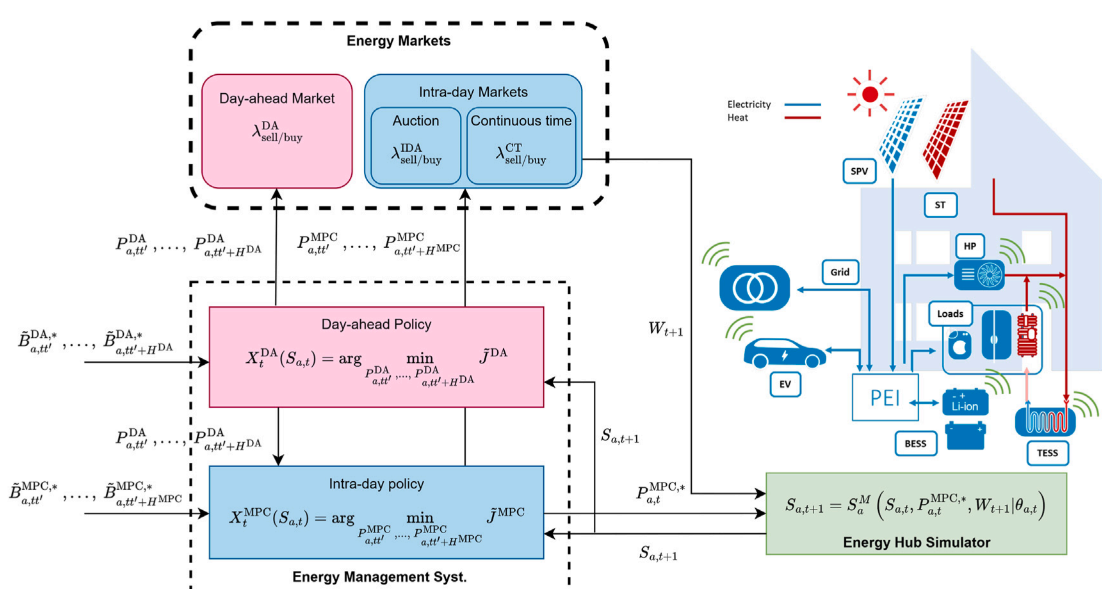

Fig. 1. Schematic diagram of the proposed electrified multi-carrier building participating in sequential energy markets.

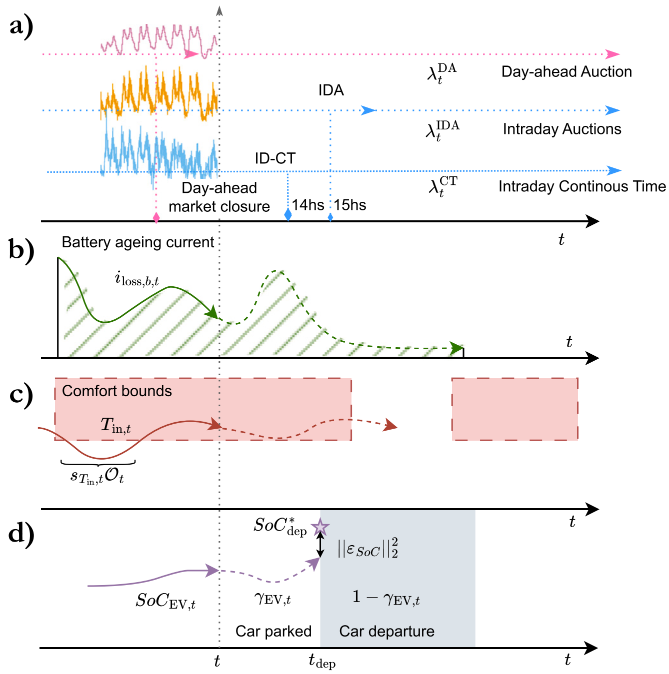

Fig. 2. Components of the cost function: a) grid cost C_{grid}, b) battery degradation cost C_{loss}, c) thermal comfort penalty p_T and d) electric vehicle charging penalty p_{SoCDep}.

only one IDA is used, and the CT order book is approximated through the ID1 index, which is the average of all transactions in the order book for the last hour.

The second component is the battery degradation cost C_{loss}. For each battery b a capacity fade current $i_{\mathrm{loss},b,t}$ represents how many Ah are lost per unit time per cell. Assuming that all cells are perfectly balanced, each pack has $N_{s,b}$ cells in series per branch and $N_{p,b}$ branches in parallel, the total degradation is defined as:

$$C_{\mathrm{loss}} = w_{\mathrm{loss}} . c_{\mathrm{loss}} . \sum_{t=0}^{T} \sum_{b} N_{\mathrm{s},b} N_{\mathrm{p},b} i_{\mathrm{loss},b,t} . \Delta t, \ \forall\ b \subset a, \tag{3}$$

The marginal cost is $c_{\mathrm{loss}} = 1.2$ €/Ah [41], and a weight w_{loss} for tuning, scaling and blending all components together.

The third objective is the user's thermal comfort. The building's internal temperature $T_{\mathrm{in},t}$ has to be kept within bounds $\underline{T}_{\mathrm{in}}, \overline{T}_{\mathrm{in}}$ while the building is occupied. Any excursion outside these bounds should be penalized. A slack variable $s_{T_{in},t}$ is defined to measure temperature excursions and the goal is to minimize it over time as in:

$$s_{T_{in},t} = \max\left(0, \max\left(\underline{T}_{\mathrm{in}} - T_{\mathrm{in},t}, T_{\mathrm{in},t} - \overline{T}_{\mathrm{in}}\right)\right) \tag{4a}$$

$$p_T = w_T \sum_{t=0}^{T} s_{T_{\mathrm{in}},t} . \mathcal{O}_t . \Delta t, \tag{4b}$$

The building occupancy is $\mathcal{O}_t$ defined as 1 for t when there's someone inside the building and 0 when nobody is.

Lastly, the EV must have enough energy to drive while it's away from home. The user defines a setpoint for departure SoC^*_{dep} and the EV has to reach it at departure time t_{dep}. The measure to be minimized is then the distance between $SoC_{\mathrm{EV},t_{\mathrm{dep}}}$ and SoC^*_{dep}, weighted by w_{SoC}:

$$\varepsilon_{SoC} = SoC_{\mathrm{EV},t_{\mathrm{dep}}} - SoC^*_{\mathrm{dep}} \tag{5a}$$

$$p_{\mathrm{SoCDep}} = w_{SoC} . ||\varepsilon_{SoC}||_2^2, \tag{5b}$$

Following the definitions in [45] the state vector has physical measurements $R_{a,t}$ and beliefs $\tilde{B}_{a,t}$ that approximate the exogenous process W_{t+1} as $S_{a,t} = [R_a, \tilde{B}_a]_t^T$, with $\tilde{B}_{a,t} = [\tilde{G}_{\mathrm{ir}}, \tilde{\gamma}_{\mathrm{EV}}, \tilde{P}_{\mathrm{load}}, \tilde{\mathcal{O}}, \tilde{T}_{\mathrm{amb}}]_t^T$. The actions or decision variables are $x^*_{a,t} = [P_{\mathrm{EV}}, P_{\mathrm{BESS}}, P_{\mathrm{HP}}, \dot{Q}^{\mathrm{D}}_{\mathrm{HP}}, \dot{Q}^{\mathrm{D}}_{\mathrm{TESS}}]_t^T$. Both the actions and state vectors have upper and lower limits denoted as $\overline{x}^*_{a,t}$, $\underline{x}^*_{a,t}$, $\overline{S}_{a,t}$, and $\underline{S}_{a,t}$. To account for converter efficiencies η_a, bidirectional powers, either actions or states, are modeled as $P_{a,t} = \eta_a P^+_{a,t} - \frac{1}{\eta_a} P^-_{a,t}$, and complementarity constraints $P^+_a \perp P^-_a$.

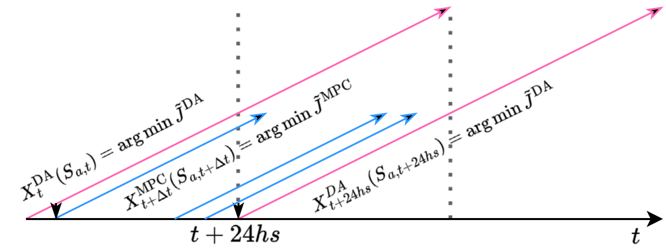

Fig. 3. Deterministic DLA seq. policy with a day-ahead planner and an MPC.

4. Policy design

The SPD in Eq. (1) is a state-dependent problem where current states influence future decisions. To solve such SPD a hierarchical policy π is proposed. The process is shown in Fig. 3 and explained in Algorithm 1. Two policies are sequentially applied, first a day-ahead policy X_t^{DA} offers a 24hr schedule for the day-ahead market $\mathcal{P}^{\mathrm{DA}}_{a,[t,t+24]}$, after Δt an eMPC policy $X^{\mathrm{MPC}}_{t+\Delta t}$ updates the DA setpoint with the new information (forecasts, states, etc.), placing a bid in the intra-day market. This updated setpoint is implemented in the real system or simulator $S^M_{a,t}$. This process is repeated every timestep until the moment of presenting a new DA schedule is reached at $t+24$hr.

The two policies are based on approximated state-space models $\tilde{S}^M_{a,t}$ of the MCES. First, the DA policy optimizes actions $P^{\mathrm{DA}}_{a,tt'}$ over the lookahead time t', with horizon H^{DA} and timestep Δt^{DA}:

$$\min_{P^{\mathrm{DA}}_{a,tt'}} \quad \tilde{J}^{\mathrm{DA}} \tag{6a}$$

$$\text{s.t.} \quad \tilde{S}^{\mathrm{DA}}_{a,tt'+1} = \tilde{S}^M_a\left(\tilde{S}^{\mathrm{DA}}_{a,tt'}, P^{\mathrm{DA}}_{a,tt'}, \tilde{B}^{\mathrm{DA}}_{tt'} | \theta_{a,tt'}\right) \tag{6b}$$

$$S\tilde{o}C^{\mathrm{DA}}_{\mathrm{BESS},tt'_1} = S\tilde{o}C^{\mathrm{DA}}_{\mathrm{BESS},tt'_1+24hs} \tag{6c}$$

Later, the eMPC optimizes actions $P^{\mathrm{MPC}}_{a,tt'}$ over the lookahead time t', with horizon H^{MPC} and timestep Δt^{MPC}:

$$\min_{P^{\mathrm{MPC}}_{a,t}} \quad \tilde{J}^{\mathrm{MPC}} \tag{7a}$$

$$\text{s.t.} \quad \tilde{S}^{\mathrm{MPC}}_{a,tt'+1} = \tilde{S}^M_a\left(\tilde{S}^{\mathrm{MPC}}_{a,tt'}, P^{\mathrm{MPC}}_{a,t}, \tilde{B}^{\mathrm{MPC}}_{tt'} | \theta_{a,tt'}\right) \tag{7b}$$

Algorithm 1 Sequential market operation algorithm.

1: **Initialize hyperparameters** Δt, $H^{\mathrm{DA/MPC}}$, w, n_d
2: **Initialize device states and inputs** $S_{a,\,0}$
3: **for** $d \in 1:n_d$ **do**
4: Solve the deterministic OCP-DA, Eq. (6), and obtain schedule $\mathcal{P}^{\mathrm{DA}}_{a,[t,H^{\mathrm{DA}}]}$.
5: **for** $t \in 0:H^{\mathrm{MPC}}$ **do**
6: Solve the deterministic OCP-CT, Eq. (7), and obtain action $P^{\mathrm{MPC}}_{a,t}$.
7: Simulate $S_{a,t+1} = S^M_{a,t}(S_{a,t}, P^{\mathrm{MPC}}_{a,t}, W_{t+1})$;
8: Update forecasts in $B^{\mathrm{MPC}}_{a,tt'}$
9: Move time window $t \leftarrow t + \Delta t^{\mathrm{MPC}}$;
10: **end for**
11: **end for**

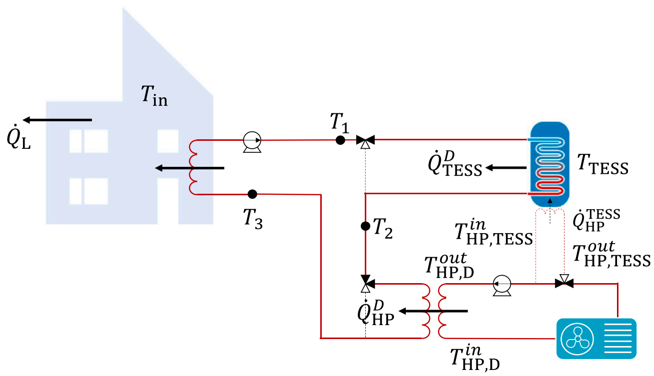

Fig. 4. Thermal heating system.

$$\tilde{SoC}^{\text{MPC}}_{\text{BESS},tt'_0} = \tilde{SoC}^{\text{MPC}}_{\text{BESS},tt'_0+H^{\text{MPC}}} \tag{7c}$$

Where both objective functions are:

$$\tilde{J}^{\text{DA/MPC}} = \tilde{C}^{\text{DA/MPC}}_{\text{grid}} + \tilde{C}^{\text{DA/MPC}}_{\text{loss}} + \tilde{p}^{\text{DA/MPC}}_{\text{SoCDep}} + \tilde{p}^{\text{DA/MPC}}_{T} \tag{8}$$

where the tilde ˜ denotes approximate, the time t is the time at which the Direct Lookahead (DLA) policy is created and t' is the time inside the policy itself and superscripts DA and MPC mark to which policy the variables correspond to. The main differences between $X^{\text{DA}}_{a,t}$ and $X^{\text{MPC}}_{a,t}$ are: their sampling frequency $\Delta t^{\text{DA}} = 1\text{hr}$ and $\Delta t^{\text{MPC}} = 15\text{min}$, their prediction horizon $H^{\text{DA}} = 48\text{hr}$ and $H^{\text{MPC}} = 24\text{hr}$, their grid cost functions $C^{\text{DA/MPC}}_{\text{grid}}$, Eqs. (2c) and (2d), and their periodicity conditions, Eqs. (6c) and (7c). These conditions mean that in the day-ahead policy X^{DA}_t solved at time t, within the lookahead time t' the $\tilde{SoC}^{\text{DA}}_{\text{BESS}}$ at policy time t'_1 has to be the same at time $t'_1 + 24\text{hr}$. Eq. (7c) means that the estimated BESS state $\tilde{SoC}^{\text{MPC}}_{\text{BESS}}$ at the initial policy time t'_0 has to be equal to the final state at the end of the horizon $t'_0 + H^{\text{MPC}}$. These two constraints are key for bounding the corresponding value functions and ensuring their bounds [51]. Combined with the optimization horizons $H^{\text{DA/MPC}}$ these ensures the turnpike properties of the controller.

The sequential deterministic optimizations approximate the true SPD in Eq. (1) by using forecasts, stored in $\tilde{B}^{\text{DA/MPC}}_{a,tt'}$, and approximated models for the transition functions $\tilde{S}^{M}_{a,t}$. The approximate transition function $\tilde{S}^{M}_{a,t}(.)$ is the compendium of the equations specified in the following sections. The controller's actions are evaluated in the true transition function $S^{M}_{a,t}$, defined in [45]. The simulator enforces all the thermal dynamics presented in Section 4.1 [31] and the battery dynamics through high-fidelity models [52]. Note the subtle difference between the approximated dynamics $\tilde{S}^{M}_{a,t}$ and the real ones $S^{M}_{a,t}$. This is not to be overlooked because the assumption that the predictions made by the policy π hold true can lead to disappointing results in real-world applications. In the future, the simulator might grow enough to be considered a digital twin of the real building.

Thus, the policies are:

$$X^{\text{DA/MPC}}_t(S_{a,t}) = \arg \min_{p^{\text{DA/MPC}}_{a,t}} \tilde{J}^{\text{DA/MPC}} \tag{9}$$

In the remainder of this section, all variables will be presented without approximations "˜" or layer superscripts DA or MPC, since all the models are present in both the EMS policies $X^{\text{DA/MPC}}_t$ and the simulator $S^{M}_{a,t}$.

4.1. Thermal carrier

4.1.1. Building

The building has an electrical heating system, presented in Fig. 4. The system comprises a HP to generate heat, a TESS to store it, and radiators to distribute it. The building loses heat $\dot{Q}_{\text{loss},t}$ through its ventilation $\dot{Q}_{\text{vent},t}$ and conduction $\dot{Q}_{\text{cond},t}$ losses. Temperature/potential-based models are used to design the controls. Another alternative is power/flow-based models such as the ones used in [45,53]. In the case of the latter, the problem becomes a scheduling problem (supply–demand matching), whereas the first option sets up a soft-tracking objective in which the building's inner temperature $T_{\text{in},t}$ is maintained within bounds, Eq. (4). The soft-tracking problem defined by temperature-based models is less computationally complex, as the defined terminal set and corresponding value function are bounded [51]. This design choice simplifies the computational complexity of the policies $X^{\text{DA/MPC}}_t(\cdot)$.

The building's thermal model dictates the evolution of its internal temperature $T_{\text{in},t}$ following a linear state-space model:

$$S_{\text{in},t} = T_{\text{in},t},\ x_{\text{in},t} = [\dot{Q}^{\text{D}}_{\text{TESS}},\ \dot{Q}^{\text{D}}_{\text{HP}}]^T_t,\ W_{\text{in},t+1} = [G_{\text{ir}},\ T_{\text{amb}}]^T_t \tag{10a}$$

$$S_{\text{in},t+1} = \mathbf{A}_{\text{in}} S_{\text{in},t} + \mathbf{B}_{\text{in}} x_{\text{in},t} + \mathbf{D}_{\text{in}} W_{\text{in},t+1} \tag{10b}$$

where $T_{\text{amb},t}$ is the ambient temperature, $G_{\text{ir},t}$ is the global irradiance, $\dot{Q}_{\text{loss},t}$ represents the losses, $\dot{Q}^{\text{D}}_{\text{TESS},t}$ is the heat supplied by the TESS to the building, $\dot{Q}^{\text{D}}_{\text{HP},t}$ is the heat supplied by the HP to the building. The losses are assumed to be linear with the temperature difference [30]. All temperatures are expressed in [K], and all heat flows are in [kW]. In the model Eq. (10), the exogenous information $W_{\text{in},t+1}$ consists of the ambient temperature $T_{\text{amb},t}$ and global irradiance $G_{\text{ir},t}$. The actions $x_{\text{in},t}$ are the heat flows $\dot{Q}^{\text{D}}_{\text{HP},t}$ and $\dot{Q}^{\text{D}}_{\text{TESS},t}$. Losses and incident radiation heat follow the models in [30,31], and are summarized in Appendix A.

4.1.2. Heat pump

An air-to-water HP generates heat from electrical power following a non-linear model [30]. The model considers complementarity between heating the TESS or the building with distinct temperatures and a non-linear coefficient of performance. The model is summarized as:

$$\dot{Q}_{\text{HP},t} = COP_t.P_{\text{HP},t}, \tag{11a}$$

$$COP_t = 7.90471.e^{-0.024.(T^{\text{in}}_{\text{HP},t} - T_{\text{amb},t})} \tag{11b}$$

$$\dot{Q}_{\text{HP},t} = \dot{Q}^{\text{TESS}}_{\text{HP},t} + \dot{Q}^{\text{D}}_{\text{HP},t} \tag{11c}$$

$$\dot{Q}^{\text{TESS}}_{\text{HP},t} \perp \dot{Q}^{\text{D}}_{\text{HP},t} \tag{11d}$$

$$T^{\text{in}}_{\text{HP,D},t} = T^{\text{out}}_{\text{HP,D},t} - \frac{\dot{Q}^{\text{D}}_{\text{HP}}}{\eta_{\text{HP}}.\dot{m}_f.c_f} \tag{11e}$$

$$T^{\text{in}}_{\text{HP, TESS},t} = T^{\text{out}}_{\text{HP, TESS},t} - \frac{\dot{Q}^{\text{TESS}}_{\text{HP}}}{\eta_{\text{HP}}.\dot{m}_f.c_f} \tag{11f}$$

$$T^{\text{in}}_{\text{HP},t} = \begin{cases} T^{\text{in}}_{\text{HP, D},t} & \dot{Q}^{\text{D}}_{\text{HP},t} \neq 0 \\ T^{\text{in}}_{\text{HP, TESS},t} & \dot{Q}^{\text{TESS}}_{\text{HP},t} \neq 0 \end{cases}. \tag{11g}$$

where $\dot{Q}_{\text{HP}}$ is the total heat produced by the HP, COP_t is the coefficient of performance, $P_{\text{HP},t}$ is the consumed electrical power, $T^{\text{in/out}}_{\text{HP},t}$ is the inlet/outlet temperature of the HP, $\dot{Q}^{\text{D}}_{\text{HP},t}$ is the heat supplied to the building, and $\dot{Q}^{\text{TESS}}_{\text{HP},t}$ is the heat supplied to the TESS. These last two are complementary with independent heat exchangers operating parallel to each other. The non-linear COP_t model, from Damianakis et al. [30], uses $T^{\text{in}}_{\text{HP},t}$ which is the corresponding heat exchanger inlet temperature, either from HP to the demand or HP to TESS. Finally, all heat flows are positive and no cooling is considered only space heating. All time-dependent variables are part of the state vector $S_{\text{HP},t}$, except for $\dot{Q}^{\text{TESS}}_{\text{HP},t}$ and $\dot{Q}^{\text{D}}_{\text{HP},t}$ which are decisions $x_{\text{HP},t}$. The rest of the parameters are in Appendix A.

4.1.3. Thermal energy storage system

This work considers an underground, perfectly mixed water tank with independent charge and discharge coils as a TESS. Assuming no mass exchange between the TESS and the piping system the TESS thermal balance is:

$$T_{\text{TESS},t+1} = T_{\text{TESS},t} + \frac{\Delta t}{m_{\text{TESS}} \cdot c_{\text{TESS}}} \left(\dot{Q}^{\text{TESS}}_{\text{HP},t} - \dot{Q}^{\text{D}}_{\text{TESS},t} - \dot{Q}_{\text{sd}} \right) \tag{12}$$

where $T_{\text{TESS},t}$ is the TESS internal temperature, $\dot{Q}_{\text{sd}}$ is the self-discharge of the TESS, m_{TESS} is the mass and c_{TESS} is the thermal capacity. Since the optimization horizons $H^{\text{DA/MPC}}$ are 1 or 2 days, the self-discharge $\dot{Q}_{\text{sd}}$ can be assumed to be a constant. To improve upon this assumption please refer to [31].

Since the tank is assumed to be perfectly mixed its $SoC_{\text{TESS},t}$ is defined by the internal temperature and its limits:

$$SoC_{\text{TESS},t} = \frac{T_{\text{TESS},t} - \underline{T}_{\text{TESS}}}{\overline{T}_{\text{TESS}} - \underline{T}_{\text{TESS}}} \tag{13}$$

Between the TESS, the building and the HP the thermal system has 2 storage devices, 1 heat source and 1 heat sink. The TESS is an active storage because both its charge and discharge are fully controllable, while the building can store energy in its heat capacity and is discharged exogenously by $\dot{Q}_{\text{loss},t}$ [28]. In combination with the controllable HP the heating is a fully flexible carrier.

4.2. Electrical carrier

In the building, all electric devices are connected through power electronic DC/DC converters at a DC bus and are connected to the LV grid through a bidirectional AC/DC converter and the building's LV switchboard through an inverter. The power balance in the DC bus is:

$$P_{\text{PV},t} + P_{\text{BESS},t} + \gamma_{\text{EV},t} . P_{\text{EV},t} + P_{\text{grid},t} = P_{\text{load},t} + P_{\text{HP},t} \, . \tag{14}$$

with the left hand side aggregating sources ($P_{\text{PV},t}, P_{\text{grid},t}$) and storage systems ($P_{\text{BESS},t}, \gamma_{\text{EV},t} . P_{\text{EV},t}$) and the right hand side aggregating the controllable ($P_{\text{HP},t}$) and uncontrollable loads ($P_{\text{load},t}$).

4.2.1. Battery energy storage system

The remaining devices in the MCES are all battery-based ESS. Batteries have complex nonlinear dynamics, and several modelling techniques are presented in the literature [37,54,55]. In this work, models derived from empirical and physics-based approaches are used, with an equivalent circuit model (ECM) for performance and a PBROM for degradation. Under the UMF, this is represented in the transition function $\tilde{S}^M_{b,t}(\tilde{S}_{b,t}, x_{b,t}, \theta_{b,t})$, which contains both the performance model $p^M_{b,t}(\cdot)$ and the ageing model $d^M_b(\cdot)$. The performance model predicts stored energy $SoC_{b,t}$ and terminal voltage $v_{t,b,t}$ and is parameterized by the parameter vector $\theta_{b,t}$. The ageing model is used to update the parameters $\theta_{b,t}$ of $p^M_{b,t}(\cdot)$, as in [45]. The degradation mechanisms to be modelled are SEI formation and active material loss (AM) which account for the majority of the battery ageing [38,43,56]. This is summarized in:

$$S_{b,t+1} = S^M_{b,t}(S_{b,t}, x_{b,t}, \theta_{b,t}) = \begin{cases} S_{b,t+1} = p^M_{b,t}\left(S_{b,t}, x_{b,t} | \theta_{b,t}\right) \\ \theta_{b,t+1} = d^M_b\left(\theta_{b,t}, S_{b,t}, x_{b,t}\right) \end{cases} \tag{15a}$$

$$S_{b,t} = \left[SoC,\ i_{R_1},\ OCV_j,\ z,\ \eta_k,\ \beta,\ i_{\text{SEI}},\ i_{\text{AM}}\right]^T_{b,t} \tag{15b}$$

$$x_{b,t} = P_{b,t},\ y_{b,t} = \left[i, v_t\right]^T_{b,t},\ \theta_{b,t} = Q_{b,t} \tag{15c}$$

The state of the battery b is composed of the state of charge SoC, the diffusion current i_{R_1}, the open circuit voltages of the electrodes OCV_j, $\forall j = n, p$, the Li stoichiometry z, the SEI kinetic overpotential η_k, the internal state β, the SEI formation rate i_{SEI}, and the active material loss of the electrodes i_{AM}. The decision variable $x_{b,t}$ is $P_{b,t}$, the available measurements y_t are the terminal voltage v_t and current i, with the ageing parameter θ_b to be optimized being the cell capacity Q. The models $p^M_{b,t}(\cdot)$ and $d^M_b(\cdot)$ are summarized in Appendix A. The used model $S^M_{b,t}(\cdot)$ assumes a constant battery temperature $T_{b,t}$ and limited C-rates, allowing us to dismiss Li-plating [38,43].

Eqs. (15) are combined with the terminal conditions Eqs. (6c) and (7c) in each corresponding policy. These terminal conditions are at the heart of this paper's contribution; ensuring the turnpike property and leading to the recursive feasibility of the 2-stage non-convex eMPC [51]. Eqs. (6c) and (7c) bound their terminal sets while ensuring enough flexibility in the controls to not fix the SoC_{BESS} at the beginning of each day.

4.2.2. Electric vehicle

The final asset in the system is the EV, which is modeled as a battery with three particularities: (i) it is not always connected to the system represented in availability $\gamma_{\text{EV},t}$, (ii) while the EV is not parked it is being driven consuming $P_{\text{drive,EV}} \sim \mathcal{N}(\mu_d, \sigma_d)$, (iii) at the time of departure the user requires it to be at a desired setpoint $SoC_{\text{EV},t_{\text{dep}}} \approx SoC^*_{\text{dep}}$, Eq. (5), as in [57]. The complete model can be found in Appendix A.

4.3. Commentary

In summary, both policies have four major goals to be fulfilled simultaneously: obtain the best economic outcome $C^{\text{DA/MPC}}_{\text{grid}}$, with the least degradation $C^{\text{DA/MPC}}_{\text{loss}}$, while charging the EV $p^{\text{DA/MPC}}_{\text{SoCDep}}$ and maintaining a comfortable inside temperature $p^{\text{DA/MPC}}_T$. The first two could be

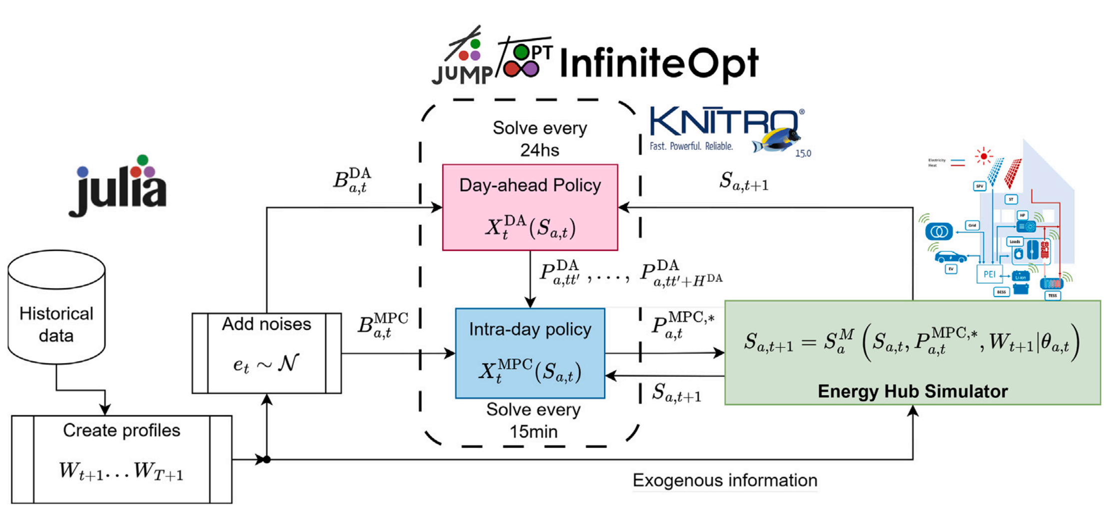

Fig. 5. Flow chart of the simulations.

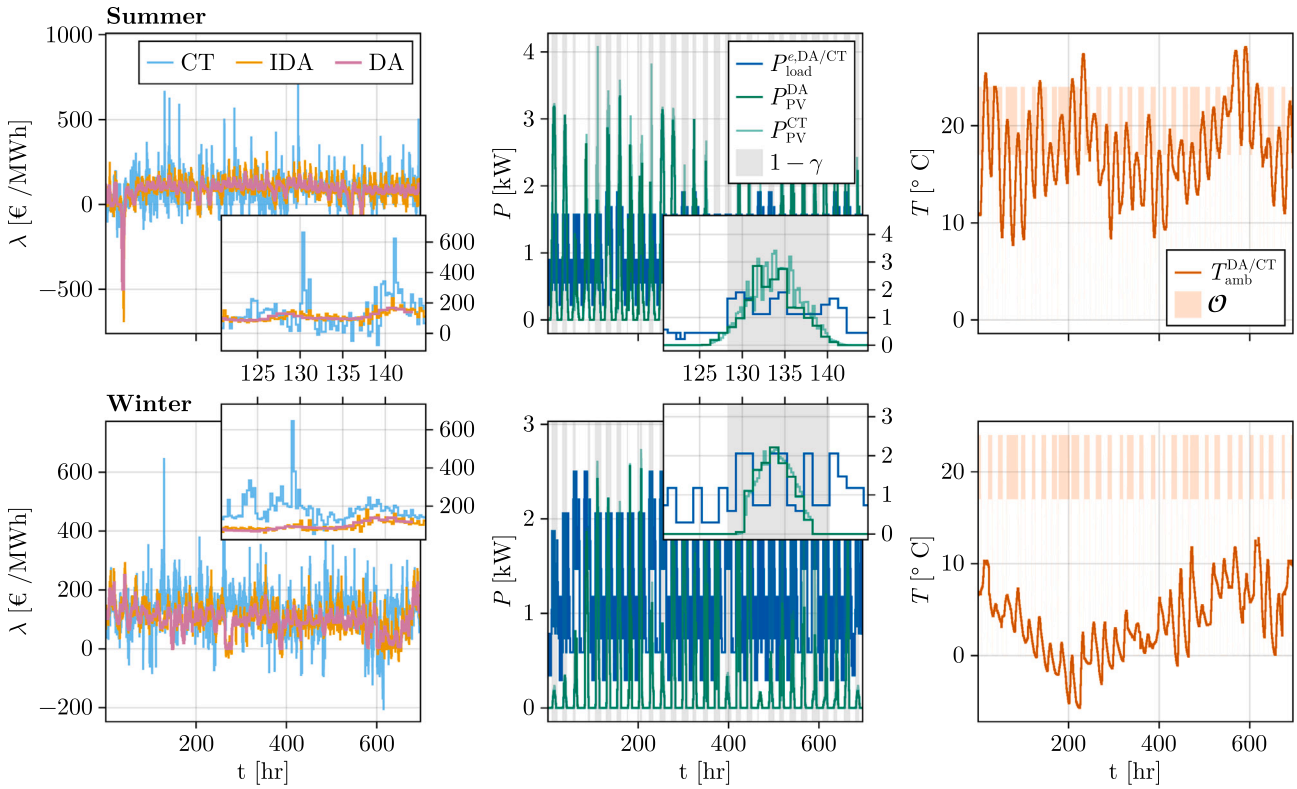

Fig. 6. Inputs for standard months. Summer (top), winter (bottom). From left to right: market prices λ_t, electric load $P^{e}_{load,t}$, solar generation $P_{PV,t}$, car availability $\gamma_{EV,t}$, ambient temperature $T_{amb,t}$, and building occupancy $\mathcal{O}_t$.

identified as scheduling problems and the second two are soft-tracking problems [51]. The terminal conditions used on the BESS are used to bound costs $J^{DA/MPC}$, accelerating convergence and avoiding the need for longer horizons [51,58]. Practically, the terminal constraints are never reached since they always lie outside of the implemented horizon, for both DA and MPC. On the same note, the policy X^{MPC}_t always has to be warm-started with either the DA prediction (if it's the first of the day) or the previous step prediction X^{MPC}_{t-1}. This ensures convergence to local optimality within reasonable times and, more importantly, recursive feasibility [51,59].

5. Case studies

The system is composed of a 4kWp solar photovoltaic (SPV), a 15.6kWh BESS, a 55.6kWh EV with nickel manganese cobalt oxide (NMC) cells, one 12.5kW EV charging point, a 5kWe heat pump, a 200kWh TESS, a 2.5kWp electrical load, and 17kW LV grid connection. Power consumption profiles (P_{load}) were constructed using data from 2021 to 2023 from TU Delft's Green Village smart meter data [60]. The output of the SPV is taken from [61–63], the market prices λ are taken from the EPEX day-ahead and intra-day markets, with $\lambda^{DA}_{sell} = 0.95\lambda^{DA}_{buy}$ and $\lambda^{MPC}_{sell} = 0.8\lambda^{MPC}_{buy}$ [48], and the ambient temperature from [64].

The cells used are NMC SANYO NCR18650 cells [43,52]. The ECM was constructed following [55]. For the thermal models, the parameters are taken from Damianakis et al. [30] with the exception of s_b and r_b for the summer, when $s_b = 0.1$ and $r_b = 0.99$ meaning that the house is properly ventilated and shaded.

The simulations were modelled and run using Julia [65], JuMP [66], and InfiniteOpt [67]. The chosen solver was KNITRO from Artelys [59]. All simulations were run using an Intel CPU at 2.60GHz, 4 processors, and 32GB of RAM. Since this is a non-linear non-convex eMPC, global optimality cannot be generally guaranteed [51,68]. Having this in mind, the implementation of the EMS approaches this limitation by: (i) using warm-starts as an initial guess to ensure convergence to the same local optima, (ii) solving day-ahead scheduling with interior point and sequential quadratic programming for the MPC layer, (iii) using the KNITRO tuner and multi-start in each individual step to increase the chance of finding the best local optima [59].

The previously mentioned components are combined following the simulation workflow presented in Fig. 5. For each simulation time window $\mathcal{D}_t$, historical data is used to generate different profiles (daily, weekly, etc.) of exogenous information W_{t+1}, which is later passed to the optimization and simulation models. Before being passed to the policies $X^{DA/MPC}_t(\cdot)$, noise e_t can be added to simulate a forecast. Once the models are built, for each time $t \in \mathcal{D}_t$ the corresponding policies $X^{DA/MPC}_t(\cdot)$ are solved and evaluated in $S^M_{a,t}(\cdot)$. The simulator feeds back the state $S_{a,t+1}$ to the policies and continues with the loop. The base library for building and simulating EMS policies is open-source and free to use in https://github.com/DarioSlaifsteinSk/EMSmodule.

5.1. Market participation and operational flexibility

The first contribution of this paper is to challenge common price assumptions in sequential market models. Usually, the literature [12–14] presents intra-day prices λ^{CT}_t as a scaled signal of the day-ahead prices λ^{DA}_t. However, participating in the intra-day auctions can be beneficial under specific circumstances. These auctions follow a pay-as-clear price λ^{IDA}_t with their own particular dynamics. This work is based on historical prices from the Netherlands, rather than the assumptions in the literature.

Fig. 6 presents the standard months for summer and winter of 2023. The first column to the left presents the day-ahead price λ^{DA}_t, the intra-day auction price λ^{IDA}_t, and the continuous-time intra-day index ID1 λ^{CT}_t. This last one is the average price of all transactions in the CT intra-day for the past hour. All three prices exhibit distinct frequency harmonics and volatility, contradicting the standard literature assumption [47].

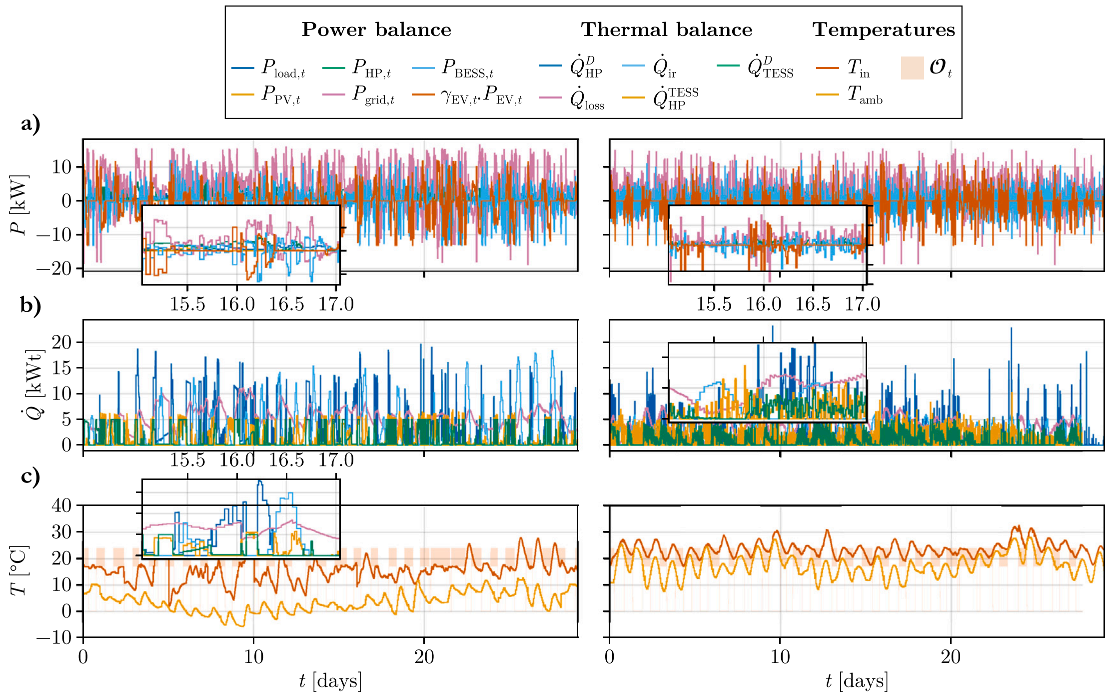

Fig. 7. Summary of the π_{DA2} monthly simulations (left) winter and (right) summer. a) Power Balance. b) Heat balance. c) Building temperatures. Inset plots zoom in on days 15 to 17.

When talking about volatility, this work refers to the standard deviation σ and peak values λ_{pk} of a given price λ_t.

In reality, an operator has to choose how much power is bid in each energy market, with the day-ahead and intra-day auctions being only financial markets. This means that it is not mandatory to dispatch the system following the bids made, but it is mandatory to deliver/receive the contracted euros €. Not following the promised power dispatch only increases risk exposure in the subsequent balancing markets, which are outside the scope of this paper.

To assess how market participation interacts with the flexibility provided by each asset, different cost function combinations are tested:

- $DA \rightarrow DA$: π_{DA2} both cost functions $J^{\text{DA/MPC}}$ follow λ^{DA}_t, with their ΔP_g evaluated against λ^{CT}_t.
- $DA \rightarrow CT$: $\pi_{DA\rightarrow CT}$ each cost function $J^{\text{DA/MPC}}$ follows $\lambda^{\text{DA/CT}}_t$, with λ^{CT}_t being the ID1 index, assuming it is a good approximation of the pay-as-bid mechanism.
- $DA \rightarrow IDA$: $\pi_{DA\rightarrow IDA}$ same as $\pi_{DA\rightarrow CT}$, but the intra-day prices are λ^{IDA}_t.
- $DA + IDA \rightarrow IDA$: π_{DA2IDA} The day-ahead optimization incorporates the dispatch of the IDA. Thus, the day-ahead dispatch contemplates the IDA as in $\tilde{J}^{\text{DA}} = \tilde{C}^{\text{DA}}_{\text{grid}} + \tilde{C}^{\text{IDA}}_{\text{grid}} + \tilde{C}^{\text{DA}}_{\text{loss}} + \tilde{p}^{\text{DA}}_{\text{SoCDep}} + \tilde{p}^{\text{DA}}_{T}$. The J^{MPC} remains the same as in $\pi_{DA\rightarrow IDA}$.

Along with the market participation, different sets of flexibility were tested. Each case is tested under perfect forecast conditions, and thus, the difference in grid costs between each case represents the value of the flexibility provided for the current set of prices. The different cases of flexibility are:

- *noFlex*, no flexibility with only PV-HP-EV.
- *thFlex*, thermal flexibility with PV-HP-TESS-EV.
- *eFlex*, electric flexibility with PV-HP-BESS-EV.
- *fullFlex*, multi-carrier flexibility with all PV-HP-BESS-EV-TESS.

For the cases *noFlex* and *thFlex* the EV is on a fast charging mode, i.e. no V2G. This means $\tilde{p}^{\text{DA/MPC}}_{\text{SoCDep}} = w_{SoC} \cdot \gamma_{\text{EV}} \cdot \sum_{t=t'}^{t'+H^{\text{DA/MPC}}} ||\tilde{SoC}^{\text{DA/MPC}}_{\text{EV},t} - SoC^{*}_{\text{dep}}||^2_2 . \Delta t$ and the discharging power is fixed to $P^{+}_{\text{EV}} = 0$.

All controllers effectively control the system, maintaining $T_{\text{in},t}$ within bounds, charging the EV close to SoC^{*}_{dep} at departure, and minimizing its own grid cost C_{grid}. As a representative example, Fig. 7 shows the dispatch of the π_{DA2} in the *fullFlex* case for the representative months of winter (left) and summer (right). From top to bottom, the first row presents the power balance, the second the heat balance, and the last one the building temperatures. From the power balance, it is clear that the EV is the most critical electrical asset due to its capacity and power, followed by the BESS. The EV is correctly charged before departure, and the BESS is used to arbitrage energy following the frequencies of the λ^{IDA}_t. Moving down to the heat balance, in summer, the TESS charges power from solar to avoid heating the house or low-value sales. In winter, the demand is supplied by HP and TESS with the latter oscillating between 50–60°. On the bottom, the evolution of the $T_{\text{in},t}$ is presented. In summer, the temperature $T_{\text{in},t}$ is close to the upper bound $\overline{T}_{\text{in}}$ when the building is occupied. Whereas, in winter $T_{\text{in},t}$ sits closer to the lower bound $\underline{T}_{\text{in}}$. The house is, in fact, also a passive thermal storage, being heated during low energy prices. This does not always coincide with the building being occupied. The rest of the *fullFlex* results for the remaining policies can be found in Appendix B.

All policies have reasonable computational times Δ_{comp} with a mean μ_{Δ} =7-15s and a standard deviation σ_{Δ} =12-47s. The computational time Δ_{comp} includes optimization, simulation and utilities, with the simulation having the highest share. More detailed information on the computational load can be found in Appendix B.

Fig. 8 presents the grid costs C_{grid} of each flexibility setup for each policy π. When comparing across markets and flexibilities, there is no policy π that comes up on top across flexibilities and seasons. The predictive policy π_{DA2IDA} achieves the lowest C_{grid} for the *noflex* setup. The *thflex* setup provides flexibility only during summer for the first three policies, while during the winter it adds C_{grid}. The *eFlex* setup achieves the lowest grid cost for all policies π with the exception of $\pi_{DA\rightarrow IDA}$ in the summer.

Particularly, the π_{DA2IDA} policy has the best day-ahead costs $C^{\text{DA}}_{\text{grid}}$ due to offering $P^{\text{DA}}_{\text{grid},t}$ beyond what is physically available to later take

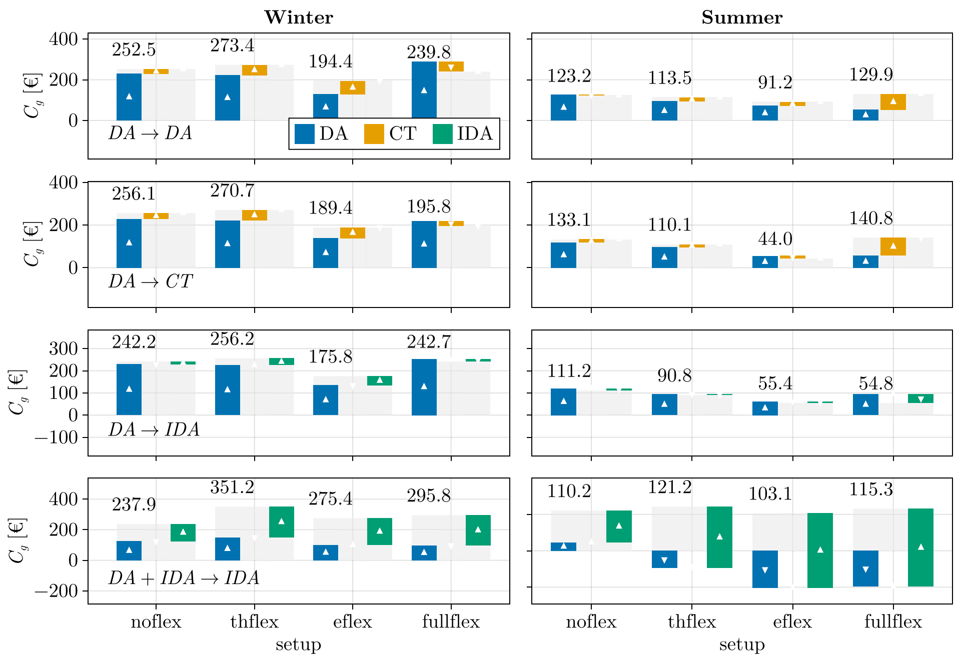

Fig. 8. Grid flexibility provided per setup and market. For winter (left), and summer (right).

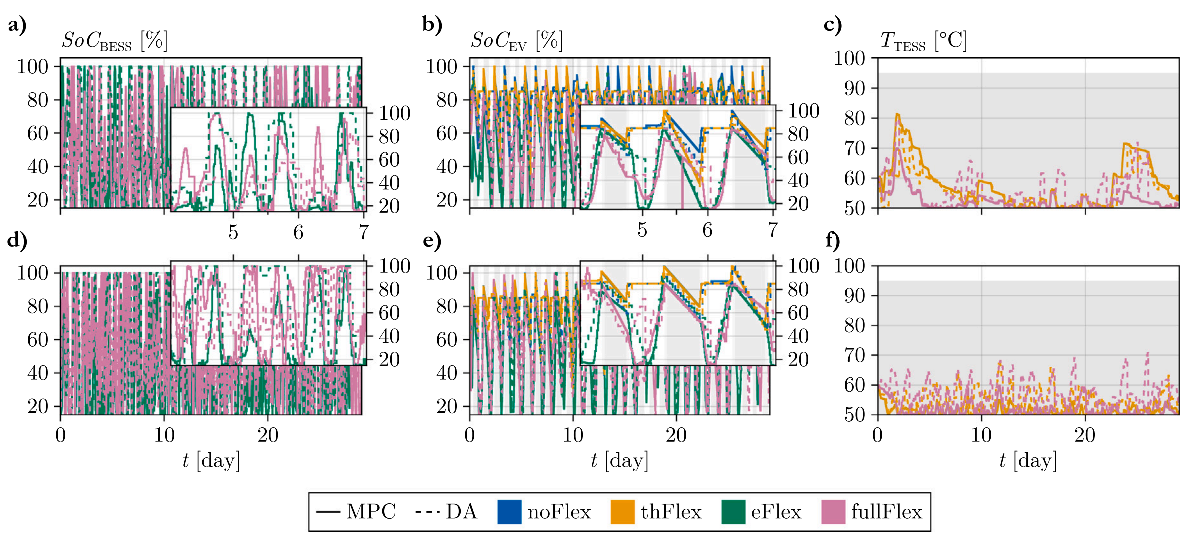

Fig. 9. HESS states under the $\pi_{DA\rightarrow IDA}$ in summer (a-c) winter (d-f) for DA plan and MPC realization. a,d) BESS State of Charge, b,e) EV State of Charge and c,f) TESS Temperature.

losses in the $C^{\text{IDA}}_{\text{grid}}$. Since in π_{DA2IDA} the grid power is $P_{\text{grid},t} = P^{\text{DA}}_{\text{grid},t} + P^{\text{IDA}}_{\text{grid},t}$, with its corresponding costs, and $\lambda^{\text{DA}}_t > \lambda^{\text{IDA}}_t$ most of the time the policy chooses to maximize $P^{\text{DA},-}_{\text{grid},t}$ and maintain a reasonable overall $P_{\text{grid},t}$. Later, in the X^{MPC}_t grid power is $P_{\text{grid},t} = P^{\text{IDA}}_{\text{grid},t}$ warm-started with the sequence decided by X^{DA}_{t-1}, leading to high intra-day auction cost $C^{\text{IDA}}_{\text{grid}}$ for the system (monetary losses). In other words, the policy π_{DA2IDA} tries to game the two markets, DA and IDA, by predicting the price auctions λ^{IDA}_t in the first stage but fails when the dataset is very diverse (high price volatility and large ambient temperature variations). In preliminary weekly simulations where price volatility and temperature variations were limited, this policy was the top performer.

Continuing, not all policies π can decrease C_{grid} when passing from *eFlex* to *fullFlex*, and even when they do, the change is marginal. The *fullFlex* setup only achieves lower C_{grid} in the summer $\pi_{DA\rightarrow IDA}$ because it already saves costs in the *thflex* setup. The TESS by itself only provides short-term flexibility in the first three policies of the summer. The main limitations are a combination of: (i) the TESS maximum heat-flow $\bar{Q}_{\text{TESS}} = 5kWth$ is smaller than the HP $\bar{Q}_{\text{HP}} = 20kWth$, (ii) the complementarity between heating the TESS or the building, Eq. (11)(d), and (iii) the H^{MPC} not being long enough to capture the value of the TESS. These will be further explained in the following sections.

The rationale behind the effectiveness of *eFlex* is that the volatility of $\lambda^{\text{DA/CT}}_t$ allows the BESS to arbitrage energy throughout the day, capturing fast price spikes and dips. The total grid cost significantly decreases when the BESS is introduced and the bidirectional charging is allowed (*eFlex* and *fullFlex*). Summarizing, the worst performing policy seems to be π_{DA2}, unaware of the IDA and CT markets. Integrating the TESS and the electric storage unlocks value only under specific conditions. The only policy that ensures the synergy between TESS and ESS is the

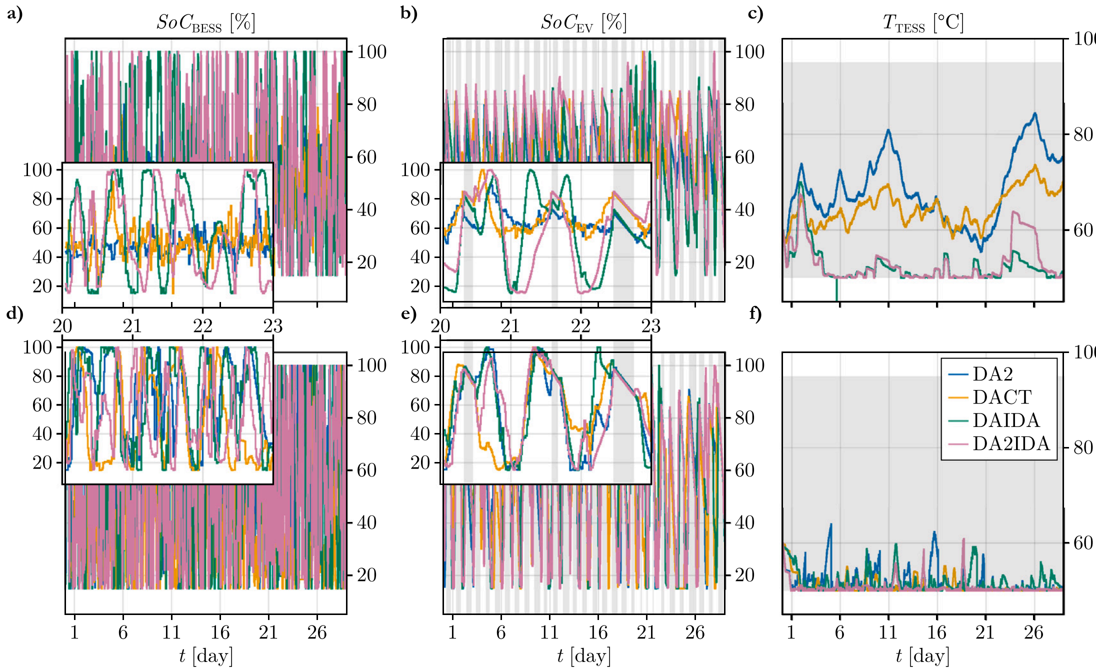

Fig. 10. Monthly HESS dispatch in the *fullFlex* case. Summer (a-c), winter (d-f), BESS State of Charge (a,d), EV State of Charge (b,e), TESS Temperature (c,f).

$\pi_{DA\rightarrow IDA}$. The statistical validation of the TESS short-term flexibility is further explored in Section 5.4.

5.2. HESS operation: from plan to execution

Moving to the HESS states, there are relevant differences between the DA plans X_t^{DA} and the implemented MPC actions X_t^{MPC}. The $\pi_{DA\rightarrow IDA}$ is used as a representative example in Fig. 9. From left to right, the $SoC_{\mathrm{BESS},t}$, Fig. 9a,d, changes its periodicity from DA to MPC, due to the higher frequency component of the intra-day prices $\lambda_t^{\mathrm{IDA/CT}}$. This is measured in full equivalent cycles FEC_{BESS} which increase between 30–60% in the winter depending on the flexibility setup. The inset presents a close-up of the end of the first week, to appreciate the difference between $\tilde{SoC}^{\mathrm{DA}}_{\mathrm{BESS},t}$ and $SoC_{\mathrm{BESS},t}$. The peaks and cycles planned by X_t^{DA} are replaced by irregular charge/discharge cycles to compensate for the variations in W_{t+1} (mainly λ_t^{MPC} and $P_{\mathrm{PV},t}$) and the incoming information at the tail of the horizon $H^{\mathrm{MPC}}+1$. The change in frequency from DA to MPC affects the other storages with less noticeable effects. The impact on EV and TESS is limited because both are tied to other demands (mobility and heating). Even though the EV is the preferred ESS due to its high round-trip efficiency and large capacity, it cannot compensate for the short-term variations because it is not always connected and it has to be charged before departure. Thus, for the BESS there are few qualitative differences between *eFlex* and *fullFlex*, with the biggest impact coming from the change between DA to MPC. For the EV the trajectories are consistent throughout seasons, and policies.

Finally, the TESS reduces its flexibility supply from DA to MPC, quantified by the decrease in full equivalent cycles FEC_{TESS}. This is partially due to the shorter horizon H^{MPC} w.r.t. H^{DA}, resulting in a greedier policy for the TESS. Greedier, meaning discharging without recharging. In the summer, the $\tilde{T}^{\mathrm{DA}}_{\mathrm{TESS},t}$ captures the negative prices from λ_t^{DA}, which is mitigated in $T_{\mathrm{TESS},t}$. As mentioned earlier, although temperature-based models offer a computational advantage over flow-based models, they do not completely address the early depletion of thermal storage. The reasons for this are three: (i) the shorter the opt. horizon H the less attractive is the flexibility of the TESS (low η, high Q, high $\dot{Q}_{\mathrm{sd}}$) [69,70], (ii) the thermal setup (complementarity and series connection) and (iii) the fact that TESS flexibility mostly causes C_{grid} savings since there is no heat-to-power and negative prices can be captured by other ESS or the building. This is a shortcoming of the chosen policy (H^{MPC}) and the design assumptions (series connection and complementarity) since some form of seasonal information could inform daily decisions or a change in the setup design, and it is an open point for further research [70]. Summarizing, from DA to MPC the increase in charge–discharge cycles is absorbed by the electrical storage (BESS and EV) and decreased in the TESS.

On a broader scope for all market sequences, the HESS operation in the *fullFlex* case is presented in Fig. 10. All the different price signals λ_t have different frequency spectra, with the CT having the largest volatility, followed by IDA and DA last. As the EV and TESS are constrained, the high efficiency BESS is always available to accommodate changes in W_{t+1}. For the EV, the main difference is the moments in which power is discharged. All policies have roughly the same FEC_{EV}, with the difference being less than a cycle. However, when zooming into the end of the 3rd week, in summer, policies π_{DA2} and $\pi_{DA\rightarrow CT}$ produce smaller $SoC_{b,t}$ deviations than the $\pi_{DA\rightarrow IDA}$ and π_{DA2IDA} policies, Figs. 10(a),b. On the thermal side, the TESS temperature in winter is brought down to its lower limit and flexibly operates within the bottom 10° C, Fig. 10(f), similar to the results presented in [45]. However, in Fig. 10(c) $T_{\mathrm{TESS},t}$ trajectories of policies π_{DA2} and $\pi_{DA\rightarrow CT}$ are consistently higher than the sequential policies trajectories, causing their high C_{grid} in Fig. 8.

The change in total FEC of the ESS from DA to MPC for all flexibilities and market combinations is presented in Table 2. In the *noFlex* and *thFlex* cases, the $\Delta FEC = \Delta FEC_{\mathrm{EV}} \leq 10\%$ meaning there is no relevant difference in the EV cycles from DA to MPC. Significant variation is introduced in *eFlex* and *fullFlex* with the BESS and the EV smart bidirectional charging. The difference between $\lambda_t^{\mathrm{DA}} \rightarrow \lambda_t^{\mathrm{CT}}$ and $\lambda_t^{\mathrm{DA}} \rightarrow \lambda_t^{\mathrm{IDA}}$ increases in the summer, leading to an increase of more than 50% in all *eFlex* cases. Whereas in winter, the change in Ah processed is less than 10%. In the *fullFlex* setups the throughput increases between 16% to almost 50%. This is because the TESS does not realize the FEC expected by X_t^{DA}, meaning the BESS and EV have to compensate for it. In general, the increase from DA to MPC realization is due to the higher short-term volatility of λ_t^{CT} and λ_t^{IDA} with respect to λ_t^{DA}. The worst case is $\pi_{DA\rightarrow CT}$ in *eFlex* during the summer with almost a 67% increase, due

Table 2
Change in FEC from DA plan to MPC realization for all markets and flexibilities.

	Winter				Summer			
	DA2	DACT	DAIDA	DA2IDA	DA2	DACT	DAIDA	DA2IDA
noflex	-6%	-6%	-6%	-10%	-12%	-10%	-11%	-13%
thflex	-2%	-2%	-4%	-3%	-4%	-5%	-5%	-5%
eflex	3%	4%	10%	6%	50%	67%	54%	47%
fullflex	27%	46%	48%	22%	16%	30%	46%	47%

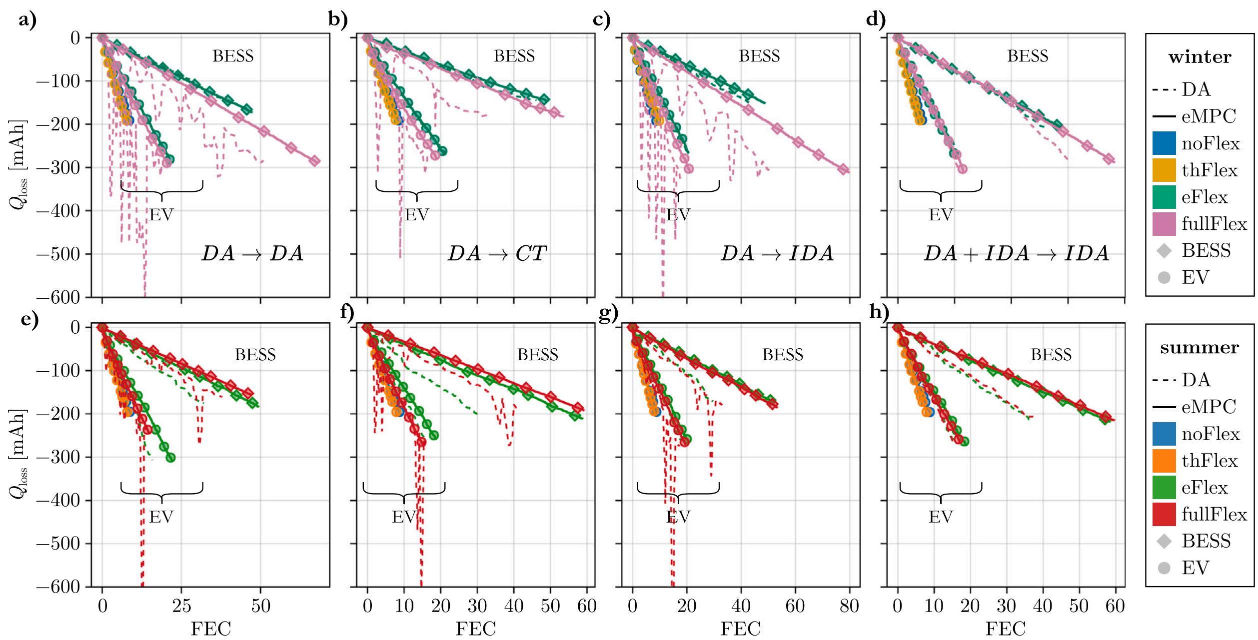

Fig. 11. Degradation trajectories for the different policies (from left to right), winter (a-d), summer (e-h).

to the increased volatility from $\lambda_t^{\mathrm{DA}} \rightarrow \lambda_t^{\mathrm{CT}}$. But how does this increased throughput impact battery degradation? A deeper analysis of this is presented in the following Section 5.3.

5.3. Battery degradation

Regarding battery degradation, Fig. 11 summarizes the impact of the different policies on the ESS. It presents the lost capacity $Q_{\mathrm{loss},b,t}$ as a function of $FEC_{b,t}$ where $b \in$ [BESS, EV]. An effective policy π would steer the trajectories to the top-right, maximizing $FEC_{b,t}$ with minimum $Q_{\mathrm{loss},b,t}$. On the contrary, an ineffective policy would steer the system towards the bottom-left corner, maximum degradation with minimum throughput. In general, the DA predictions are always below the MPC realization $\tilde{Q}^{\mathrm{DA}}_{\mathrm{loss},T} < Q_{\mathrm{loss},T}$ due to the increase in $F\tilde{E}C^{\mathrm{DA}}_{b,T} < FEC_{b,T}$. The transition from *eFlex* to *fullFlex* leads to different results depending on the season. In the winter, all *fullFlex* BESS trajectories have steeper degradation control ($\frac{\partial Q_{\mathrm{loss,BESS},t}}{\partial FEC_{\mathrm{BESS},t}}$), whereas in the summer this only happens with $\pi_{DA\rightarrow IDA}$. For the other three policies in the summer, the slope decreases, meaning that degradation control improves with the addition of the TESS. The $Q_{\mathrm{loss,EV},t}$ value is roughly the same for *eFlex* and *fullFlex* across different seasons and policies. Coincidentally, in the summer Figs. 11(e)-h, the addition of the TESS leads to higher C_{grid} but also to lower Q_{loss} in all policies **except for $\pi_{DA\rightarrow IDA}$ which lowers its grid cost but loses more capacity**. This is because the addition of the TESS sometimes causes the solver to find a different local minima where the BESS is cycled less, reducing its cyclic ageing. The downside of this is that in those occasions the flexibility is reduced (i.e., an increase in C_{grid} when *eFlex* → *fullFlex*). Quantitatively, the policies with the least degradation per cycle (smallest $\frac{\partial Q_{\mathrm{loss},t}}{\partial FEC_t}$) are the π_{DA2} and π_{DA2IDA} ranging from **6.4 to 6.9 mAh per eq. cycle**, which coincidentally had the highest grid costs C_{grid}.

Overall, the cause of the degradation control is the ageing PBROM, because it directly relates battery current $i_{b,t}$ with the capacity fade $Q_{\mathrm{loss},b,t}$ in a dynamic manner. This creates schedules where the cycles capture value while protecting battery lifetime [33,37,71]. Another relevant phenomenon is the fact that since the batteries are at the beginning of their lifetime, the calendar ageing factor of the SEI model is dominant versus the cyclic component. This leads the policies π to increase FEC since the final Q_{loss} will stay roughly the same. In other words, the BESS and EV will degrade anyway, so it's better to cycle them. Flexibility and degradation control meet at Table 3, which presents the ratio between the flexibility gained ΔC_{grid} and the total capacity lost Q_{loss}, i.e., how much flexibility was lost/gained by each lost mAh of storage capacity. Even though the *eFlex* cases of the sequential policies $\pi_{DA\rightarrow CT}$ and $\pi_{DA\rightarrow IDA}$ spend their mAh more wisely than their counterparts, the policies with the best degradation control are π_{DA2} and π_{DA2IDA}.

The total degradation is controllable by means of w_{loss}. As an example, Fig. 12 presents the sensitivity of the total capacity fade Q_{loss} against w_{loss} for the *eFlex* setup in standard weeks ($T = 7$ days) of summer and winter. As expected, as w_{loss} increases the capacity fade is reduced. The pattern is nonlinear, which is natural given that the batteries used are at the beginning of their lifetime and that the optimization problem is numerically scaled at each timestep. This leads to a range ($w_{\mathrm{loss}} \in [0.01, 10]$) where $Q_{\mathrm{loss},T}$ is roughly constant, where the calendar ageing dominates with respect to the cyclic ageing, since the former depends on $\sqrt{t}$. This calendar component presents a higher slope w.r.t. the cyclic components of $i_{\mathrm{SEI},t}$ and $i_{\mathrm{AM},t}$. As the weight increases past the breaking point, the capacity fade is reduced by decreasing the $SoC_{b,t}$ as

Table 3
Grid cost savings per unit of lost battery capacity [€/mAh] for all markets and flexibilities relative to their *noflex* setup.

	Winter				Summer			
	DA2	DACT	DAIDA	DA2IDA	DA2	DACT	DAIDA	DA2IDA
noflex	-	-	-	-	-	-	-	-
thflex	-0,11	-0,07	0,00	0,00	0,05	0,11	0,10	-0,05
eflex	0,13	0,16	0,16	-0,08	0,06	0,19	0,13	0,01
fullflex	0,02	0,13	-0,00	-0,10	-0,02	-0,02	0,12	-0,01

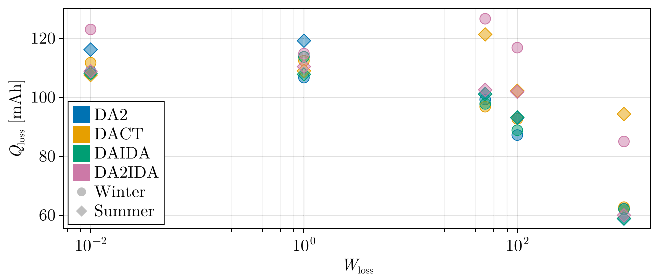

Fig. 12. Total capacity fade Q_{loss} of *eFlex* under different policies π for standard weeks ($T = 1$ week).

much as possible and by reducing the EV V2G service. As a caveat, since the knee-point is around $w_{\text{loss}} = 500$ the impact on the other objectives, it is not straightforward. As w_{loss} increases, it becomes comparable to the thermal comfort penalty p_T and the EV charging penalty p_{SoCDep}. Thus, a priori, the increase in w_{loss} only ensures a decrease in Q_{loss}, not a direct increase in grid cost C_{grid}. For example, for $w_{\text{loss}} = 1000$ there are local solutions with extended battery lifetime and relatively low grid cost, but at the expense of not charging the EV or heating the house. Thus, for each new w_{loss} a new set of weights for the penalties needs to be found, as it is usual in optimization problems with weighted-sum objectives. As the calendar degradation component naturally decreases, the sensitivity range becomes wider and reduces this effect. For further details, please refer to [43,44,56].

5.4. Noisy performance

Finally, the same *fullFlex* case is tested under noisy conditions at a noise level of 10% for the summer and winter standard weeks. Each policy is tested under $N_s = 50$ realizations of the exogenous processes $W_{t+1} \in \Omega$. Each forecast realization/trajectory is defined as $\tilde{B}_{tt'+1,\omega} = W_{t+1} + \epsilon_{t,\omega}$ with $\omega \in [1, N_s]$ being the realization index and $\epsilon_{t,\omega} \sim \mathcal{N}(0,\sigma)$ a white noise with standard dev./noise level σ. In summary, at each timestep t the policy π receives a noisy forecast $\tilde{B}_{tt'+1,\omega}$ optimizes over t' and is evaluated in the simulator under the test data W_{t+1}.

The grid cost distributions are shown in Fig. 13 for the *fullFlex* case under all policies, except for the π_{DA2IDA} since it has proven to become fragile under diverse operating conditions. From Fig. 13, we see that π_{DA2} is the riskiest policy, having the most cases with higher C_{grid}. The best policy seems to be $\pi_{DA\to IDA}$ in both seasons, with the distribution further to the left. This is due to the particular statistics of each market signal. Since the original λ_t^{DA} degrades the most when introducing noise $\epsilon_{t,\omega}$, following the noisy signal $W_{t+1} + \epsilon_{t,\omega}$ results in the worst performance. On the other end, the λ_t^{IDA} is usually below the λ_t^{DA}, thus the cases where the noisy forecast overestimates DA and underestimates IDA result in unexpected gains for the $\pi_{DA\to IDA}$ because the spread between IDA and DA is smaller than expected, allowing the policy to buy lower than expected in the DA market and sell higher than expected in the IDA.

The impact of uncertainty on the degradation of the battery storage depends on the market sequence, presented in Fig. 14. For the EVs the FEC are tightly coupled to the true $P_{\text{drive},t}$ and $\gamma_{\text{EV},t}$, as such the small variation on $FEC_{\text{EV},T}$ explained on the noisy forecast $\hat{P}_{\text{drive},t}$ and $\hat{\gamma}_{\text{EV},t}$ that generates volatility on the $SoC_{\text{EV},t}$. The closer the $SoC_{\text{EV},t}$ is to its lower bound $\underline{SoC}_{\text{EV}}$ the smaller the capacity fade $Q_{\text{loss,EV},T}$. In other words, incorrectly forecasting mobility demand leads to low $SoC_{\text{EV},t}$ results in smaller degradation, but at the risk of running out of battery in the middle of a trip. On the other hand, the BESS has almost a $\Delta FEC_{\text{BESS},T} \approx 50\%$ variation due to poor forecasting. However, as opposed to the EV, since the BESS is always available, the policies achieve a lower $\frac{\partial Q_{\text{loss}}}{\partial FEC}$/improved degradation control. When comparing the policies to each other, the policy π_{DA2} has the overall worst degradation control/steepest $\frac{\partial Q_{\text{loss}}}{\partial FEC}$ in both seasons. Finally, there is no significant difference between the other two policies, with the $\pi_{DA\to IDA}$ being better positioned since its distribution of C_{grid} has the lowest value at risk.

Summarizing, in this Section, it has been shown how the proposed novel two-layer eMPC participates sequentially in the day-ahead and intra-day markets. From the power balance, the EV and the BESS are the most critical electrical assets. While the EV has limited flexibility because it has to be charged before departure, the BESS is used to arbitrage energy following the frequencies of the $\lambda_t^{\text{IDA/CT}}$. On the heat side, the TESS delivers power until it gets close to $\underline{T}_{\text{TESS}}$ and struggles to be an attractive short-term flexibility provider when compared to electrical storage and under the series setup assumed in this work. Moreover, not all policies π ensure a decrease in C_{grid} when adding the TESS.

Lastly, when analyzing the effectiveness of the capacity fade control, it is clear that stacking markets in general increases the total capacity lost Q_{loss}. However, in most cases, moving from DA to CT or IDA increases the quality of the degradation control by reducing the capacity lost per full equivalent cycle. Within these two groups of policies can be distinguished: π_{DA2} and π_{DA2IDA} focus on extending battery lifetime, whereas $\pi_{DA\to CT}$ and $\pi_{DA\to IDA}$ spend their degradation more effectively to improve the flexibility of the residential energy hub.

5.5. Limitations & discussion

Accurate forecasting of all **exogenous processes** (W_{t+1}) is a prerequisite for effective operation, which requires $B_{a,t} \approx W_{t+1}$. In particular, predicting the clearing price for the pay-as-clear IDA market is simpler than estimating the dynamic distribution of the pay-as-bid CT market. This difficulty is compounded by the modelling assumption that the CT market functions as a **pay-as-clear auction** based on the ID1 index. Conversely, certain binary exogenous variables, such as EV availability ($\gamma_{\text{EV},t}$) and building occupancy ($\mathcal{O}_t$), are often estimated directly from user input or pre-set schedules, offering a more readily available, albeit still imperfect, set of inputs for the EMS. Finally, weather forecasts can be fetched through APIs from KNMI, data retailers, or developed in-house.

For experimental implementation, the system needs state observers to accurately feed back the current device states ($S_{a,t}$) to the control policies (π). This is essential for the closed-loop functionality of the EMS. Furthermore, several simplifying assumptions were made regarding the thermal behavior of energy storage devices. Specifically, both the BESS and the EV battery are assumed to maintain a constant operating temperature, implying HVAC systems for both. This assumption simplifies the control problem by neglecting the nonlinear effects of temperature

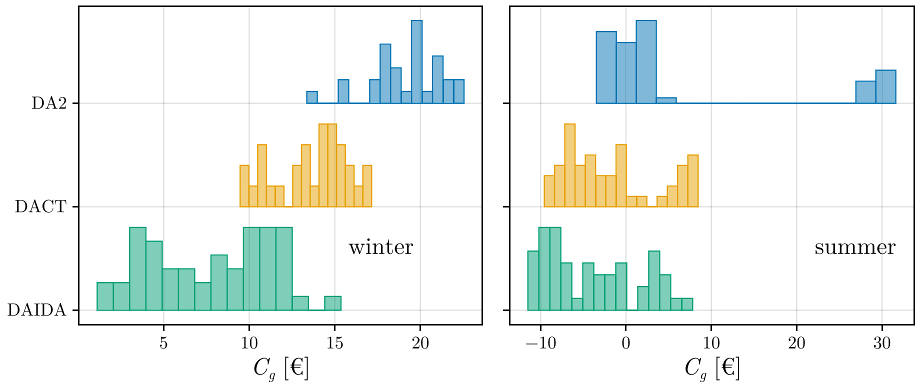

Fig. 13. Grid costs distributions of *fullfFlex* under noisy conditions for weekly simulations.

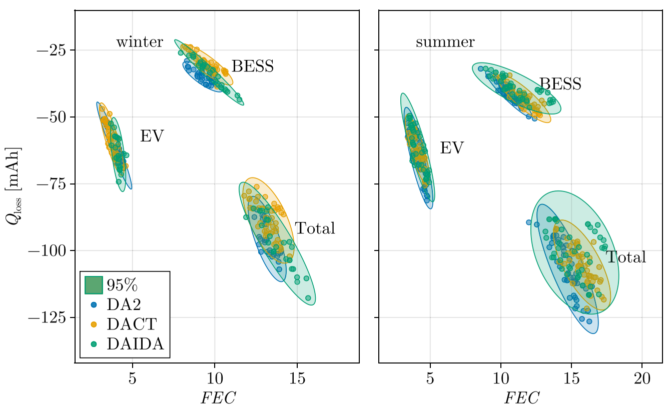

Fig. 14. Final degradation distributions for each policy under noisy conditions.

on battery degradation and performance. In combination with the limited C-rates, Li-plating is also neglected, but future work should aim to incorporate temperature controls and additional battery degradation mechanisms, especially for countries with harsher weather conditions like snow and extreme heat.

Despite efforts to improve flexibility compared to standard literature, the terminal set design remains somewhat arbitrary. Future work should focus on designing the terminal conditions (Eqs. (6c) and (7c)) using a more rigorous and systematic criterion to enhance the stability and optimality of the long-term control horizon. More so when thinking that due to the short MPC horizon the TESS flexibility is marginal, even hindering the overall flexibility as price volatility and test set heterogeneity grow. This trade-off between long-term operation, short-term flexibility and TESS appears as an interesting research direction.

As mentioned earlier, this work aims to challenge existing literature assumptions regarding the impact of sequential markets on energy hubs. This is manifested in the higher harmonic content of $\lambda_t^{\mathrm{IDA/CT}}$ w.r.t λ_t^{DA}, which results in increased Q_{loss}, something previously not analyzed in the literature. Batteries exposed to sequential market operations will require adequate mitigation measures to control their degradation, driving the need for innovative business models not only for individual homes but for aggregated schemes. This type of consideration wouldn't be possible without the use of advanced control-oriented battery PBROM [33]. Their adoption in more applications is a critical step for the massive adoption of battery technologies to assess revenues, warranties, and lifetimes with a broader lens.

Of course, it is highly unlikely that a single house has all the devices necessary for *fullFlex* and with current market structures the business case for a single household is quite challenging. However, this paper shows that without specialized cloud-infrastructure or prohibitive computation hardware a *fullFlex* ageing-aware eMPC can be implemented in remote-servers in under Δt^{MPC} =15min since the mean computational time is μ_Δ < 2min. Thus, the potential for aggregators to optimize behind the meter assets is significant. Moreover a roadmap for gradual implementation is given, since the short-term flexibility contribution is presented with the logical steps being *noflex* → *eFlex* → *fullFlex*. On the infrastructure side, communication can be implemented over traditional protocols such as Modbus TCP or specialized data layers like S2 or OpenADR [72], depending on the available engineering hours.

Overall, the variation between the different policies π is the price signals that they follow. As the volatility of such signals increases ($DA \rightarrow IDA \rightarrow CT$) in the short term the electrical storage is best suited to exploit it. To integrate the TESS into the *eFlex* setup and become *fullFlex* the volatility and heterogeneity of W_{t+1} has to be reduced or broken down by decomposition techniques, special-warm starts or new thermal setup designs.

6. Conclusions

In summary, this paper presents a two-stage economic model predictive controller for residential energy hubs. The eMPC can actively control battery ageing and thermal comfort through detailed physics-based models, while optimizing grid costs and charging the EV. The presented formulation can be integrated into day-ahead and intra-day markets (auctions and continuous-time), not only optimizing the day-ahead market, but also sequentially optimizing multiple markets.

Focusing on the grid cost C_{grid}, our analysis shows that under sequential markets, the worst policy is to follow only the day-ahead prices π_{DA2} or try to anticipate the IDA with π_{DA2IDA} if the operating conditions W_{t+1} are too heterogeneous. On the contrary, the best policy is optimizing for day-ahead and intra-day auction prices the BESS and EV. During winter, or moments when W_{t+1} resembles winter, it is best following day-ahead and then any intra-day market ($\pi_{DA\rightarrow IDA/CT}$). For summer, it is best to follow the continuous time intra-day instead of the auction ($\pi_{DA\rightarrow CT}$) which exploits the duck curves of $\lambda_t^{\mathrm{DA/CT}}$. Unfortunately, integrating TESS with BESS and EV under CT hinders the flexibility of the energy hub. These contradict the common literature assumption that always following λ_t^{CT} is the best possible policy. If the focus is on extending battery lifetime, following the intra-day auction ($\pi_{DA\rightarrow IDA}$) is the top-performing policy, because it achieves the least possible capacity fade. Moreover, preliminary degradation analysis where only DA market participation is considered does not reflect the effective degradation achieved during implementation under sequential energy markets, since the full equivalent cycles of the batteries increase from DA to CT or IDA.

Regarding the flexibility of the setup, the first case study presents the limited synergies between the heat and power storage. Our findings show that the integration of the TESS with the BESS and EV unlocks additional savings mainly in the day-ahead market. However, TESS flexibility is only delivered under specific policies and input conditions. Only in summer with the IDA policy $\pi_{DA\to IDA}$. However, its total short-term realized flexibility is marginal when compared to BESS and EV with bi-directional charging. The limiting factors are the assumed thermal piping, the TESS low round-trip efficiency and low C-rate. This is inline with current literature [31,70]. The incorporation of the TESS impacts battery degradation differently depending on the season. In the winter, the capacity lost increases for both BESS and EV. For both, the addition of the TESS hinders the ageing control (increases $\frac{\partial Q_{\text{loss}}}{\partial FEC}$).

In general, participating in sequential markets increases the overall degradation of the batteries due to the higher volatility of the intra-day markets, which is usually overlooked in the literature and by the manufacturers. Degradation controls are crucial to mitigate this additional capacity fade. In this line, the sequential policies $\pi_{DA\to CT}$ and $\pi_{DA\to IDA}$ are the most effective at converting lost battery capacity into short-term flexibility.

Future works aim at integrating the presented policies with local real-time controls and observers. A seasonal-planning layer to improve the coordination with the heat carrier and avoid the early depletion of the thermal storage is also attractive. Another direction is the explicit integration of exogenous uncertainty W_{t+1} into the policy design. Finally, the addition of other relevant markets, such as frequency reserves and similar, also appears as an attractive future research directions.

CRediT authorship contribution statement

Darío Slaifstein: Writing – review & editing, Writing – original draft, Visualization, Validation, Software, Resources, Methodology, Investigation, Formal analysis, Data curation, Conceptualization. **Gautham Ram Chandra Mouli**: Writing – review & editing, Supervision, Project administration. **Laura Ramirez-Elizondo**: Supervision. **Pavol Bauer**: Supervision, Project administration.

Declaration of competing interest

The authors declare the following financial interests/personal relationships which may be considered as potential competing interests:

Dario Slaifstein reports that financial support was provided by the Ministry of Economic Affairs and Climate Policy. If there are other authors, they declare that they have no known competing financial interests or personal relationships that could have appeared to influence the work reported in this paper.

Acknowledgment

The project was carried out with a Top Sector Energy subsidy from the Ministry of Economic Affairs and Climate, administered by the Netherlands Enterprise Agency (RVO). The specific subsidy for this project pertains to the MOOI subsidy round 2020.

Appendix A. Parameters and models

See Table A.4.

A.1. Thermal models

Building model

$$T_{\text{in},t+1} = T_{\text{in},t} + \frac{\Delta t}{C_b + V_b.\rho_{\text{air}}.C_{\text{air}}}\left(\dot{Q}_{\text{ir},t} + \dot{Q}^{\text{D}}_{\text{TESS},t} + \dot{Q}^{\text{D}}_{\text{HP},t} - \dot{Q}_{\text{loss},t}\right) \quad \text{(A.1a)}$$

$$\dot{Q}_{\text{ir},t} = w_b.s_b.G_{\text{ir},t}.\sum_{s=2}^{3} A_s \quad \text{(A.1b)}$$

$$\dot{Q}_{\text{loss},t} = \dot{Q}_{\text{cond},t} + \dot{Q}_{\text{vent},t} \quad \text{(A.1c)}$$

$$\dot{Q}_{\text{vent},t} = C_{\text{air},t}.\rho_{\text{air}}.V_b.r_b.(T_{\text{in},t} - T_{\text{amb},t}) \quad \text{(A.1d)}$$

$$\dot{Q}_{\text{cond},t} = (T_{\text{in},t} - T_{\text{amb},t})\sum_{s=1}^{S} U_s.A_s \quad \text{(A.1e)}$$

Table A.4
Parameter values for the building.

Parameter	Symbol	Unit	Value Winter	Summer
Air capacity	C_{air}	$\frac{\text{kWh}}{\text{kg.K}}$	0.279×10^{-3}	
Air density	ρ_{air}	$\frac{\text{kg}}{\text{m}^3}$	1.225	
Building thermal capacity	C_b	$\frac{\text{kWh}}{\text{K}}$	4.755	
Building volume	V_b	m^3	585	
Windows solar heat gain coefficient	s_b	–	0.5	0.1
Building wall-to-wall ratio	w_b	–	0.3	
Air change rate	r_b	$\frac{1}{\text{h}}$	0.35	0.99
Thickness of the surfaces	d	m	[0.03, 0.23, 0.23, 0.015]	
Conductivity of the surfaces	U	$\frac{\text{kW}}{\text{m.K}}$	$[0.18, 1., 1., 0.72] \times 10^{-3}$	
Area of the surfaces	A	m^2	[90., 75., 48., 63.75]	
Mass flow of the fluid	$\dot{m}_f$	$\frac{\text{kg}}{\text{s}}$	0.22	
Specific heat capacity of the fluid	c_f	$\frac{\text{kWh}}{\text{kg.K}}$	1.16×10^{-3}	
HP Heat-exchanger thermal efficiency	η_{HP}	–	0.8	
Supply temperature setpoint	T_{sup}	K	323	
Building temperature bounds	$\underline{T}_{\text{in}}$, $\overline{T}_{\text{in}}$	K	[290, 297]	

TESS self-discharge $\dot{Q}_{\text{sd}} = 1\%$ of the capacity Q_{TESS}.

A.2. Electrical models

Battery models

$$SoC_{b,t+1} = SoC_{b,t} - \frac{\Delta t}{Q_{b,t}.3600}.\eta_c.i_{b,t} \quad \text{(A.2a)}$$

$$P_{b,t} = N_{s,b}.N_{p,b}.v_{t,b,t}.i_{b,t} \quad \text{(A.2b)}$$

$$i_{R_1,b,t+1} = e^{-\frac{\Delta t}{R_{1,b}.C_{1,b}}}.i_{R_1,b,t} + \left(1 - e^{-\frac{\Delta t}{R_{1,b}.C_{1,b}}}\right).i_{b,t} \quad \text{(A.2c)}$$

$$OCV_{b,t} = OCV_{p,b,t}(SoC_{b,t}) - OCV_{n,b,t}(SoC_{b,t}) \quad \text{(A.2d)}$$

$$v_{t,b,t} = OCV_{b,t} - i_{R_1,b,t}.R_{1,b} - i_{b,t}.R_{0,b} \quad \text{(A.2e)}$$

$$z_{b,t} = SoC_{b,t}.(z_{100\%} - z_{0\%}) + z_{0\%} \quad \text{(A.2f)}$$

$$\eta_{k,b,t} = \frac{2.R.T}{F}.\sinh^{-1}\left(\frac{i_{b,t}}{n_{\text{SEI}}.a_s.A.L_n.i_0}\right) \quad \text{(A.2g)}$$

$$\beta_{b,t} = e^{\frac{n_{\text{SEI}}.F}{R.T}.(\eta_{k,b,t} + OCV_{n,b,t} - OCV_s)} \quad \text{(A.2h)}$$

$$i_{\text{SEI},b,t} = \frac{k_{\text{SEI},b}.e^{\frac{-E_{\text{SEI},b}}{RT}}}{n_{\text{SEI}}.(1 + \lambda_b.\beta_{b,t}).\sqrt{t}} \quad \text{(A.2i)}$$

$$i_{\text{AM},b,t} = k_{\text{AM},b}.e^{\frac{-E_{\text{AM},b}}{R.T}}.SoC_{b,t}.|i_{b,t}|.Q_{b,0} \quad \text{(A.2j)}$$

$$i_{\text{loss},\ b,t} = i_{\text{SEI},b,t} + i_{\text{AM},b,t} \quad \text{(A.2k)}$$

$$Q_{b,t+1} = Q_{b,t} - \frac{\Delta t}{3600}.i_{\text{loss},b,t} \quad \text{(A.2l)}$$

$$S_{b,t} = \left[SoC,\ i_{R_1},\ OCV_j,\ z,\ \eta_k,\ \beta,\ i_{\text{SEI}},\ i_{\text{AM}}\right]^T_{b,t} \quad \text{(A.2m)}$$

$$x_{b,t} = P_{b,t},\ y_{b,t} = \left[i, v_t\right]^T_{b,t},\ \theta_{b,t} = Q_{b,t} \quad \text{(A.2n)}$$

Electric vehicle

$$\gamma_t = \begin{cases} 0 & t \in [t_{\text{dep}};\ t_{\text{arr}}] \\ 1 & \text{otherwise} \end{cases}. \quad \text{(A.3a)}$$

$$P_{\text{tot,EV},t} = \gamma_{\text{EV},t}.P_{\text{EV},t} + (1 - \gamma_{\text{EV},t})P_{\text{drive,EV}} \quad \text{(A.3b)}$$

$$\varepsilon_{SoC} = SoC_{\text{EV}}(t_{\text{dep}}) - SoC^*_{\text{dep}} \quad \text{(A.3c)}$$

$$p_{\text{SoCDep}} = w_{SoC}.||\varepsilon_{SoC}||_2^2 \quad \text{(A.3d)}$$

Appendix B. Extended results

The Figs. B.15–B.17 present the rest of the *fullFlex* balances and indoor temperature for the remaining policies $\pi_{DA\to IDA}$, $\pi_{DA\to CT}$ and π_{DA2IDA}.

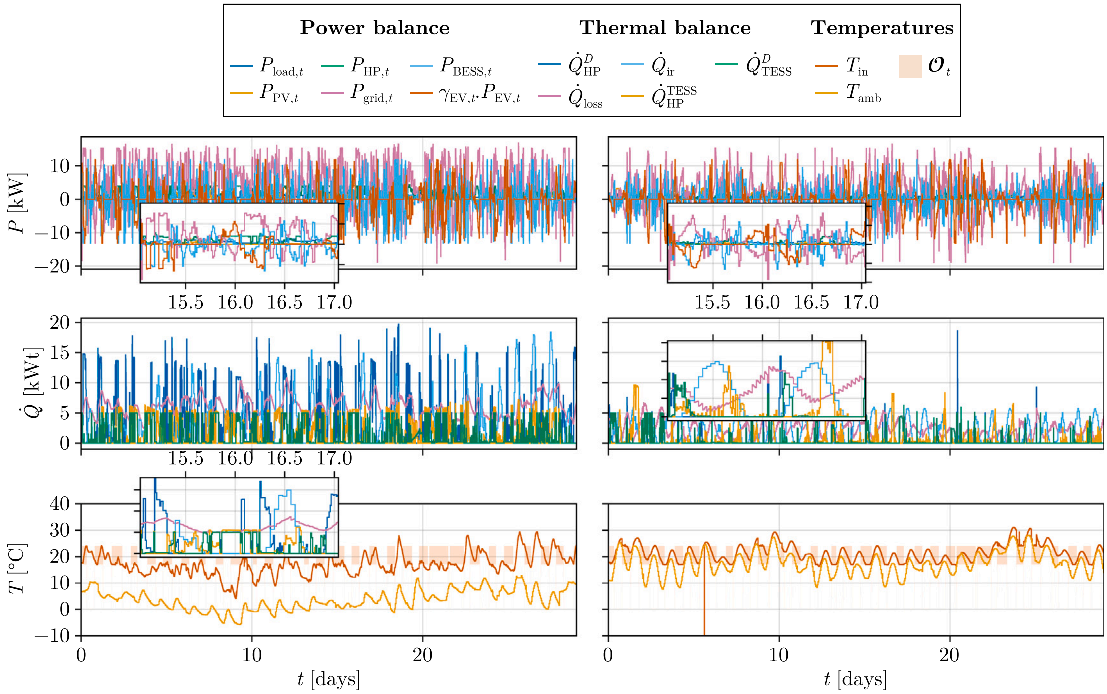

Fig. B.15. Summary of the $\pi_{DA\rightarrow IDA}$ monthly simulations, (left) winter and (right) summer. a) Power Balance. b) Heat balance. d) Building temperatures.

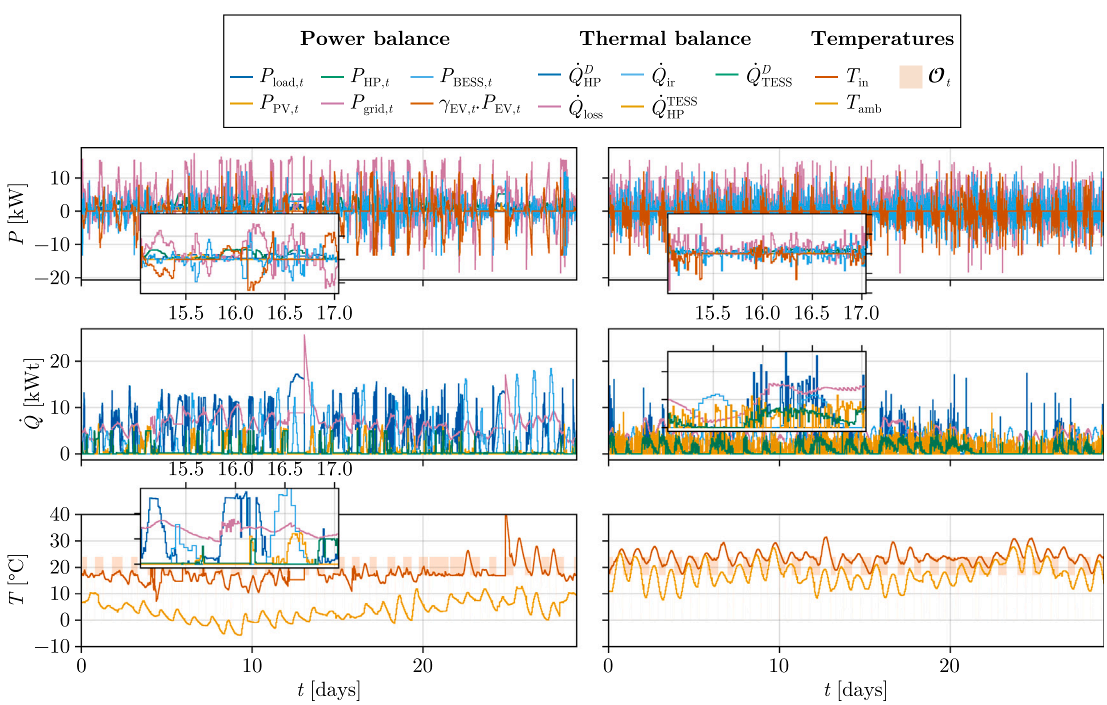

Fig. B.16. Summary of the $\pi_{DA\rightarrow CT}$ for weekly simulations, with the left column being summer and right column being winter. a) Power Balance. b) Heat balance. d) Building temperatures.

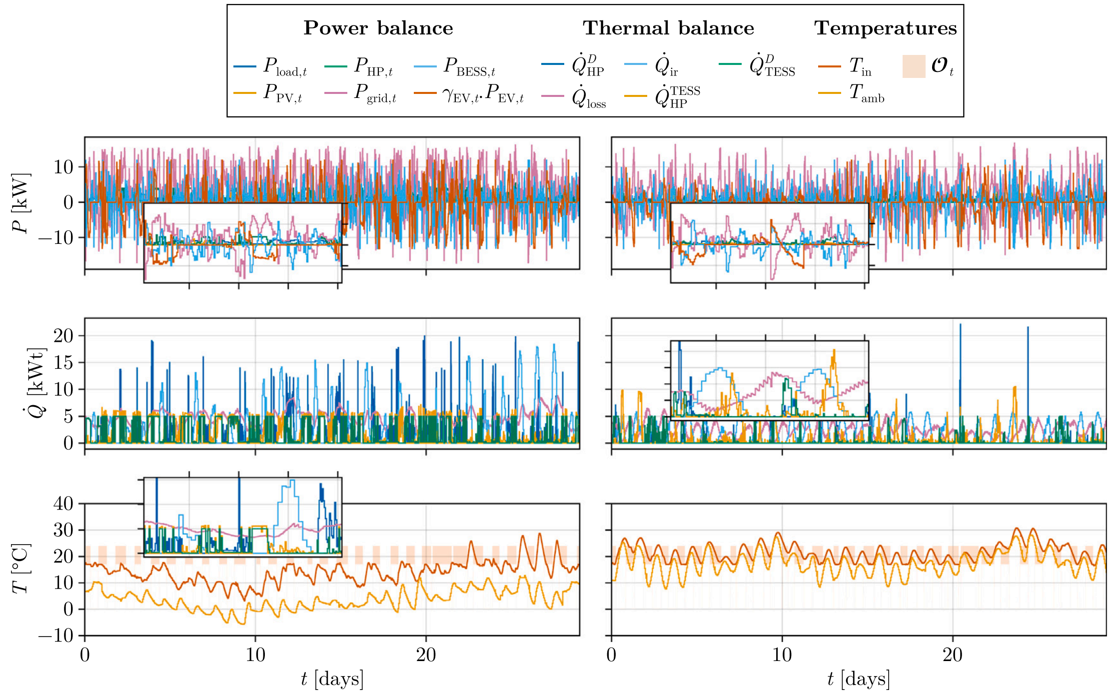

Fig. B.17. Summary of the $\pi_{DA+IDA\rightarrow IDA}$ for weekly simulations, with the left column being summer and right column being winter. a) Power Balance. b) Heat balance. d) Building temperatures.

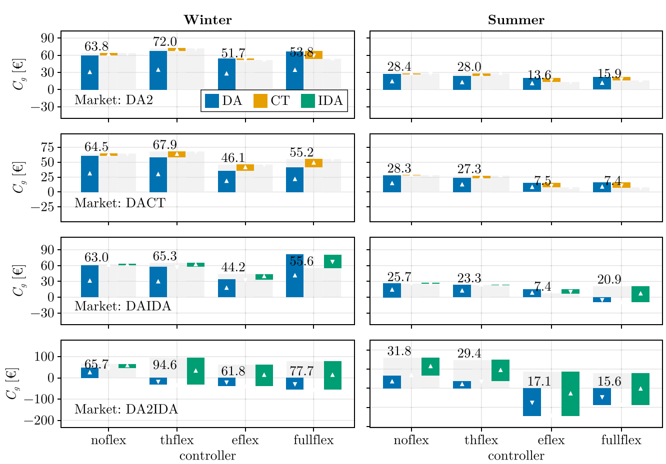

Fig. B.18. Grid flexibility provided per setup and market. For winter (left), and summer (right) and weekly standard weeks.

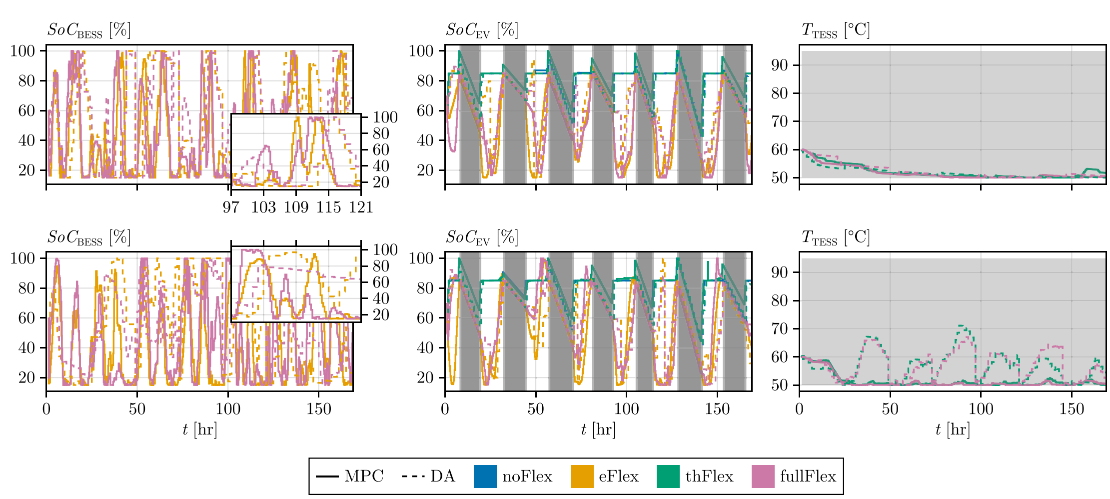

Fig. B.19. HESS states under the π_{DA2} in summer (top) winter (bottom).

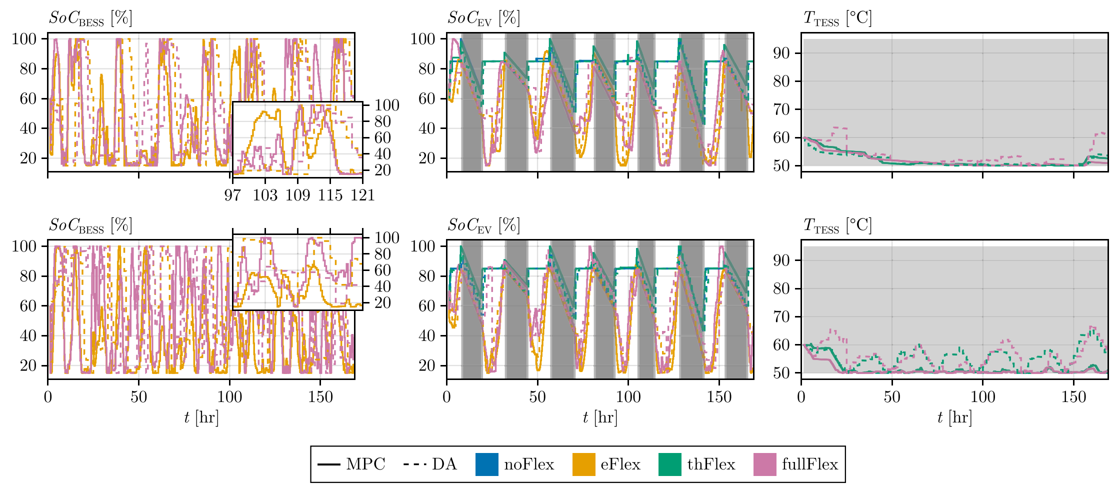

Fig. B.20. HESS states under the $\pi_{DA\rightarrow CT}$ in summer (top) winter (bottom).

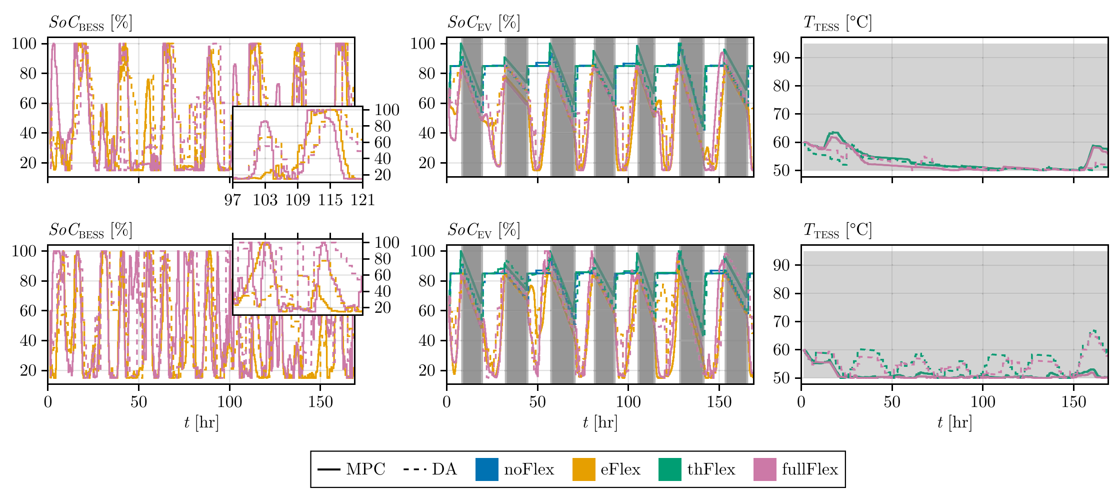

Fig. B.21. HESS states under the π_{DA2IDA} in summer (top) winter (bottom).

Table B.5
Mean and standard deviation of the computational times Δ_{comp}.

Case	Winter								Summer							
	DA2		DACT		DAIDA		DA2IDA		DA2		DACT		DAIDA		DA2IDA	
	μ	σ	μ	σ	μ	σ	μ	σ	μ	σ	μ	σ	μ	σ	μ	σ
noflex	5,85	13,84	18,024	33,1184	32,98	63,40	6,26	14,77	13,03	28,78	–		20,00	41,38	14,20	31,83
thflex	12,03	22,38	–		7,42	15,30	12,08	21,91	10,20	20,89	–		8,85	17,87	8,65	17,57
eFlex	5,97	15,87	–		6,11	11,96	12,70	15,24	9,61	18,88	–		10,99	24,48	11,61	15,36
fullFlex	25,92	89,85	–		16,07	85,53	3,76	10,04	25,55	56,56	17,28	45,9192	47,68	131,70	2,75	3,92

The Figs. B.19–B.21 present the rest of the HESS operation plots the rest of the policies π_{DA2}, $\pi_{DA\rightarrow CT}$ and π_{DA2IDA} for standard weeks $T = 1$ week. The grid costs for such standard weeks are found in Fig. B.18.

Table B.5 presents a detailed breakdown per policy and per flexibility setup of the computational times Δ_{comp}.

Data availability

Original data is confidential but processed data is shared in the following repositories: the base library can be found in https://github.com/DarioSlaifsteinSk/EMSmodule and the case studies are in https://github.com/DarioSlaifsteinSk/seqREnergyHub_eMPC.

References

[1] World energy outlook 2024 – analysis - IEA. 2024. https://www.iea.org/reports/world-energy-outlook-2024.

[2] Li R, Satchwell AJ, Finn D, Christensen H, Kummert M, Le Dréau J, Lopes RA, Madsen H, Salom J, Henze G, Wittchen K. Ten questions concerning energy flexibility in buildings. Build Environ 2022;223:109461. https://doi.org/10.1016/j.buildenv.2022.109461. http://creativecommons.org/licenses/by/4.0/.

[3] Andersson G, Zurich E, Geidl M. Optimal power dispatch and conversion in systems with multiple energy carriers PlanGridEV view project BPES-optimal sizing and control of balancing power in the future EU power system considering transmission constraints view project optimal power DISPATC. Proc 15th Power Syst Comput Conf PSCC 2005. https://www.researchgate.net/publication/228776936.

[4] Geidl M, Andersson G. Optimal power flow of multiple energy carriers. IEEE Trans Power Syst 2007;22(1):145–55. https://doi.org/10.1109/TPWRS.2006.888988. https://ieeexplore.ieee.org/document/4077107/.

[5] Vermeer W, Mouli GRC, Bauer P. Real-Time building smart charging system based on PV forecast and Li-Ion battery degradation. Energies 2020;13(13):3415. https://doi.org/10.3390/EN13133415. https://www.mdpi.com/1996-1073/13/13/3415/htm. https://www.mdpi.com/1996-1073/13/13/3415.
[6] Vermeer W, Chandra Mouli GR, Bauer P. A comprehensive review on the characteristics and modeling of Lithium-Ion battery aging. IEEE Trans on Transp Electrification 2022;8(2):2205–32. https://doi.org/10.1109/TTE.2021.3138357. https://ieeexplore.ieee.org/document/9662298/.
[7] Ceusters G, Rodríguez RC, García AB, Franke R, Deconinck G, Helsen L, Nowé A, Messagie M, Camargo LR. Model-predictive control and reinforcement learning in multi-energy system case studies. Appl Energy 2021;303:117634. https://doi.org/10.1016/j.apenergy.2021.117634. https://linkinghub.elsevier.com/retrieve/pii/S0306261921010011.
[8] Ceusters G, Camargo LR, Franke R, Nowé A, Messagie M. Safe reinforcement learning for multi-energy management systems with known constraint functions. Energy AI 2023;12:100227. https://doi.org/10.1016/j.egyai.2022.100227. https://linkinghub.elsevier.com/retrieve/pii/S2666546822000738.
[9] Van Der Meer D, Mouli GRC, Mouli GME, Elizondo LR, Bauer P. Energy management system with PV power forecast to optimally charge EVs at the workplace. IEEE Trans Ind Informatics 2018;14(1):311–20. https://doi.org/10.1109/TII.2016.2634624
[10] Ye Y, Qiu D, Wu X, Strbac G, Ward J. Model-free real-time autonomous control for a residential multi-energy system using deep reinforcement learning. IEEE Trans Smart Grid 2020;11(4):3068–82. https://doi.org/10.1109/TSG.2020.2976771. https://ieeexplore.ieee.org/document/9016168/.
[11] Esmaeel Nezhad A, Rahimnejad A, Nardelli PHJ, Gadsden SA, Sahoo S, Ghanavati F. A shrinking horizon model predictive controller for daily scheduling of home energy management systems. IEEE Access 2022;10:29716–30. https://doi.org/10.1109/ACCESS.2022.3158346. https://ieeexplore.ieee.org/document/9732346/.
[12] Jouini T, Bensmann A, Lilge T, Hanke-Rauschenbach R, Müller M. Predictive operation of Multi-Energy systems in sequential markets: a case study. In: 2024 European Control Conference (ECC). IEEE; 2024. p. 1509–15. https://doi.org/10.23919/ECC64448.2024.10591115. https://ieeexplore.ieee.org/document/10591115/.
[13] Garcia-Torres F, Bordons C, Tobajas J, Marquez JJ, Garrido-Zafra J, Moreno-Munoz A. Optimal schedule for networked microgrids under deregulated power market environment using model predictive control. IEEE Trans Smart Grid 2021;12(1):182–91. https://doi.org/10.1109/TSG.2020.3018023
[14] Li P, Guo T, Abeysekera M, Wu J, Han Z, Wang Z, Yin Y, Zhou F. Intraday multi-objective hierarchical coordinated operation of a multi-energy system. Energy 2021;228:120528. https://doi.org/10.1016/j.energy.2021.120528. https://linkinghub.elsevier.com/retrieve/pii/S0360544221007775.
[15] Zhou Y, Wei Z, Sun G, Cheung KW, Zang H, Chen S. A robust optimization approach for integrated community energy system in energy and ancillary service markets. Energy 2018;148:1–15. https://doi.org/10.1016/j.energy.2018.01.078. https://linkinghub.elsevier.com/retrieve/pii/S0360544218300963.
[16] Johnsen AG, Mitridati L, Zarrilli D, Kazempour J. The value of ancillary services for electrolyzers, arXiv (Oct, 2023). http://arxiv.org/abs/2310.04321.
[17] Schweppe FC, Caramanis MC, Tabors RD, Bohn RE. Spot pricing of electricity. Spot Pricing of Electricity 1988. https://doi.org/10.1007/978-1-4613-1683-1
[18] Ceusters G, Putratama MA, Franke R, Nowé A, Messagie M. An adaptive safety layer with hard constraints for safe reinforcement learning in multi-energy management systems. Sustain Energy Grids Netw 2023;36:101202. https://doi.org/10.1016/J.SEGAN.2023.101202
[19] Yu L, Xie W, Xie D, Zou Y, Zhang D, Sun Z, Zhang L, Zhang Y, Jiang T. Deep reinforcement learning for smart home energy management. IEEE Internet Things J 2020;7(4):2751–62. https://doi.org/10.1109/JIOT.2019.2957289
[20] Ahrarinouri M, Rastegar M, Seifi AR. Multiagent reinforcement learning for energy management in residential buildings. IEEE Trans Ind Informatics 2021;17(1):659–66. https://doi.org/10.1109/TII.2020.2977104
[21] Huang C, Zhang H, Wang L, Luo X, Song Y. Mixed deep reinforcement learning considering discrete-continuous hybrid action space for smart home energy management. J Mod Power Syst Clean Energy 2022;10(3):743–54. https://doi.org/10.35833/MPCE.2021.000394
[22] Paesschesoone S, Kayedpour N, Manna C, Crevecoeur G. Reinforcement learning for an enhanced energy flexibility controller incorporating predictive safety filter and adaptive policy updates. Appl Energy 2024;368:123507. https://doi.org/10.1016/j.apenergy.2024.123507. https://linkinghub.elsevier.com/retrieve/pii/S0306261924008900.
[23] Zhou Y, Ma Z, Zhang J, Zou S. Data-driven stochastic energy management of multi energy system using deep reinforcement learning. Energy 2022;261:125187. https://doi.org/10.1016/j.energy.2022.125187. https://linkinghub.elsevier.com/retrieve/pii/S0360544222020771.
[24] Gros S, Jakus D, Vasilj J, Zanon M. Day-ahead scheduling and real-time economic MPC of CHP unit in microgrid with smart buildings. IEEE Trans Smart Grid 2019;10(2):1992–2001. https://doi.org/10.1109/TSG.2017.2785500
[25] Vermeer W, Mouli GRC, Bauer P. Optimal sizing and control of a PV-EV-BES charging system including primary frequency control and component degradation. IEEE Open J Ind Electron Soc 2022;3:236–51. https://doi.org/10.1109/OJIES.2022.3161091. https://ieeexplore.ieee.org/document/9740621/.
[26] Rawlings JB, Mayne DQ, Diehl MM, Barbara S. Model predictive control: theory, computation, and design. 2nd ed. Nob Hill Publishing; 2022. http://www.nobhillpublishing.com.
[27] Li Y, Yang Y, Tang J, Xiong B, Deng X, Tang D. Design of degradation-conscious optimal dispatch strategy for home energy management system with rooftop PV and Lithium-Ion batteries. In: 2019 4th International Conference on Intelligent Green Building and smart Grid (IGBSG). IEEE; 2019. p. 741–6. https://doi.org/10.1109/IGBSG.2019.8886194. https://ieeexplore.ieee.org/document/8886194/.
[28] Risbeck MJ. Mixed-Integer model predictive control with applications to building energy systems [Ph.D. thesis] (2018. https://digital.library.wisc.edu/1711.dl/HYZKXNHJKGARE8C.
[29] Mariano-Hernández D, Hernández-Callejo L, Zorita-Lamadrid A, Duque-Pérez O, Santos García F. A review of strategies for building energy management system: model predictive control, demand side management, optimization, and fault detect & diagnosis. J Build Eng 2021;33:101692. https://doi.org/10.1016/J.JOBE.2020.101692
[30] Damianakis N, Mouli GCR, Bauer P. Risk-averse estimation of electric heat pump power consumption. In: 2023 IEEE 17th International Conference on Compatibility, Power Electronics and Power Engineering (CPE-POWERENG). IEEE; 2023. p. 1–6. https://doi.org/10.1109/CPE-POWERENG58103.2023.10227424. https://ieeexplore.ieee.org/document/10227424/.
[31] Alpízar-Castillo J, Ramírez-Elizondo LM, Bauer P. Modelling and evaluating different multi-carrier energy system configurations for a Dutch house. Appl Energy 2024;364:123197. https://doi.org/10.1016/j.apenergy.2024.123197. https://linkinghub.elsevier.com/retrieve/pii/S0306261924005804.
[32] Damianakis N, Mouli GRC, Yu Y, Bauer P. Coordinated power control of PV generation, electric mobility and electric heating in different grids. IEEE Int Power Electron Motion Control Conf IPEMC ECCE Asia 2024:2082–7. https://doi.org/10.1109/IPEMC-ECCEASIA60879.2024.10567854
[33] Vega–Garita V, Heydarzadeh M, Dadash AH, Immonen E. The need for aging-aware control methods in lithium-ion batteries: a review. J Energy Storage 2025;132:117653. https://doi.org/10.1016/J.EST.2025.117653. https://www.sciencedirect.com/science/article/pii/S2352152X25023667?via.
[34] O'Kane SEJ, Ai W, Madabattula G, Alonso-Alvarez D, Timms R, Sulzer V, Edge JS, Wu B, Offer GJ, Marinescu M. Lithium-ion battery degradation: how to model it. Phys Chem Chem Phys 2022;24(13):7909–22. https://doi.org/10.1039/D2CP00417H. http://xlink.rsc.org/?DOI=D2CP00417H.
[35] Prada E, Di Domenico D, Creff Y, Bernard J, Sauvant-Moynot V, Huet F. A simplified electrochemical and thermal aging model of LiFePO 4 - graphite Li-ion batteries: power and capacity fade simulations. J Electrochem Soc 2013;160(4):616–28. https://doi.org/10.1149/2.053304JES/XML. https://iopscience.iop.org/article/10.1149/2.053304jes/meta.
[36] Reniers JM, Mulder G, Howey DA. Review and performance comparison of mechanical-chemical degradation models for Lithium-Ion batteries. J Electrochem Soc 2019) A3189–A3200. 166(14). https://doi.org/10.1149/2.0281914jes. https://iopscience.iop.org/article/10.1149/2.0281914jes.
[37] Plett GL, Trimboli MS. Battery management systems. Volume III: physics-based methods. 1st ed. Norwood: Artech House; 2024. https://uk.artechhouse.com/Battery-Management-Systems-Volume-III-Physics-Based-Methods-P2201.aspx.
[38] Jin X, Vora A, Hoshing V, Saha T, Shaver G, García RE, Wasynczuk O, Varigonda S. Physically-based reduced-order capacity loss model for graphite anodes in Li-ion battery cells. J Power Sources 2017;342:750–61. https://doi.org/10.1016/j.jpowsour.2016.12.099. https://linkinghub.elsevier.com/retrieve/pii/S037877531631802X.
[39] Purewal J, Wang J, Graetz J, Soukiazian S, Tataria H, Verbrugge MW. Degradation of lithium ION batteries employing graphite negatives and nickel–cobalt–manganese oxide + spinel manganese oxide positives: part 2, chemical–mechanical degradation model. J Power Sources 2014;272:1154–61. https://doi.org/10.1016/J.JPOWSOUR.2014.07.028
[40] Xavier MA, de Souza AK, Karami K, Plett GL, Trimboli MS. A computational framework for Lithium Ion cell-level model predictive control using a physics-based reduced-order model. IEEE Control Syst Lett 2021;5(4):1387–92. https://doi.org/10.1109/LCSYS.2020.3038131. https://www.ieee.org/publications/rights/index.html. https://ieeexplore.ieee.org/document/9259035/.
[41] Reniers JM, Howey DA. Digital twin of a MWh-scale grid battery system for efficiency and degradation analysis. Appl Energy 2023;336:120774. https://doi.org/10.1016/J.APENERGY.2023.120774. https://linkinghub.elsevier.com/retrieve/pii/S0306261923001381.
[42] Reniers JM, Mulder G, Howey DA. Unlocking extra value from grid batteries using advanced models. J Power Sources 2021;487(December 2020):229355. https://doi.org/10.1016/j.jpowsour.2020.229355. https://linkinghub.elsevier.com/retrieve/pii/S0378775320316438.
[43] Jin X. Aging-aware optimal charging strategy for lithium-ion batteries: considering aging status and electro-thermal-aging dynamics. Electrochim Acta 2022;407:139651. https://doi.org/10.1016/j.electacta.2021.139651. https://linkinghub.elsevier.com/retrieve/pii/S0013468621019356.
[44] Dorronsoro X, de Castro R, Varela Barreras J, Garayalde E, Iraola U. Battery aging-aware adaptive model predictive control based on coupled semi-empirical electro-thermal and aging models. Appl Energy 2025;401:126494. https://doi.org/10.1016/J.APENERGY.2025.126494. https://www-sciencedirect-com.tudelft.idm.oclc.org/science/article/pii/S0306261925012243?getft_integrator=scopus&pes=vor&utm_source=scopus#fd0080.
[45] Slaifstein D, Ram G, Mouli C, Ramirez-Elizondo L, Bauer P. Aging-aware energy management for residential Multi-Carrier energy systems, arXiv (Mar, 2025). https://arxiv.org/abs/2503.16139v1.
[46] Hornek T, Lee Y, Menci SP, Pavić I. The value of battery energy storage in the continuous intraday market: forecast VS. Perfect foresight strategies, arXiv (Jun, 2025). http://arxiv.org/abs/2501.07121.
[47] Birkeland D, AlSkaif T, Duivenvoorden S, Meeng M, Pennings JME. Quantifying and modeling price volatility in the Dutch intraday electricity market. Energy Rep 2024;12:3830–42. https://doi.org/10.1016/j.egyr.2024.09.031. https://linkinghub.elsevier.com/retrieve/pii/S2352484724006073.

[48] EPEX spot - market data services. 2023. https://www.epexspot.com/en/marketdataservices.
[49] Powell WB. A unified framework for stochastic optimization. Eur J Oper Res 2019;275(3):795–821. https://doi.org/10.1016/J.EJOR.2018.07.014
[50] Powell W. Reinforcement learning and stochastic optimization: a unified framework for sequential decisions, vol. 22. Wiley; 2022. https://doi.org/10.1080/14697688.2022.2135456. https://www.tandfonline.com/doi/full/10.1080/14697688.2022.2135456.
[51] Grüne L, Pannek J. Nonlinear model predictive control theory and algorithms. Springer; 2017. https://doi.org/10.1007/978-3-319-46024-6. http://www.springer.com/series/61.
[52] Planden B, Lukow K, Henshall P, Collier G, Morrey D. A computationally informed realisation algorithm for lithium-ion batteries implemented with LiiBRA.jl. J Energy Storage 2022;55:105637. https://doi.org/10.1016/j.est.2022.105637. https://linkinghub.elsevier.com/retrieve/pii/S2352152X22016255.
[53] Slaifstein D, Joel Alpízar-Castillo T, Alvaro Menendez Agudin T, Laura Ramírez-Elizondo T, Ram Chandra Mouli G, Bauer P. Aging-aware battery operation for multicarrier energy systems. In: 49th annual conference of the IEEE Industrial Electronics Society (IES). Singapore; 2023.
[54] Plett GL. Battery management systems volume i battery modeling. Artech House Power Engineering and Power Electronics; 2015. https://us.artechhouse.com/Battery-Management-Systems-Volume-1-Battery-Modeling-P1752.aspx.
[55] Plett GL. BATTERY MANAGEMENT SYSTEMS volume II: Equivalent-Circuit methods. 1st ed. Artech House Power Engineering and Power Electronics; 2016. https://us.artechhouse.com/Battery-Management-Systems-Volume-II-Equivalent-Circuit-Methods-P2192.aspx.
[56] Movahedi H, Pannala S, Siegel J, Harris SJ, Howey D, Stefanopoulou A. Extra throughput versus days lost in V2G services: influence of dominant degradation mechanism. J Energy Storage 2024;104:114242. https://doi.org/10.1016/J.EST.2024.114242. https://linkinghub.elsevier.com/retrieve/pii/S2352152X24038283.
[57] Slaifstein D, Agudin AM, Mouli GRC, Ramírez-Elizondo L, Bauer P. Stochastic mobility integration into residential energy hubs. 2024 IEEE Int Conf Electr Syst Aircraft Railway Ship Propuls Road Veh Int Transp Electr Conf ESARS-ITEC 2024 2024. https://doi.org/10.1109/ESARS-ITEC60450.2024.10819794
[58] Köhler J, Müller MA, Allgöwer F. Analysis and design of model predictive control frameworks for dynamic operation—an overview. Annu Rev Control 2024;57:100929. https://doi.org/10.1016/J.ARCONTROL.2023.100929
[59] Byrd RH, Nocedal J, Waltz RA. Knitro: an integrated package for nonlinear optimization. Springer, Boston, MA; 2006. https://doi.org/10.1007/0-387-30065-1_4. http://link.springer.com/10.1007/0-387-30065-1_4.
[60] The green village, fieldlab voor duurzame innovatie. 2024. https://www.thegreenvillage.org/.
[61] Smets A, Jäger K, Isabella O, van Swaaij R, Zeman M. Solar energy: the Physics and engineering of photovoltaic conversion, technologies and systems. UIT Cambridge Ltd; 2016. https://ebookcentral-proquest-com.tudelft.idm.oclc.org/lib/delft/detail.action?docID=4781743.
[62] Diab I, Scheurwater B, Saffirio A, Chandra-Mouli GR, Bauer P. Placement and sizing of solar PV and wind systems in trolleybus grids. J Clean Prod 2022;352:131533. https://doi.org/10.1016/J.JCLEPRO.2022.131533
[63] Diab I, Saffirio A, Chandra-Mouli GR, Bauer P. A simple method for sizing and estimating the performance of PV systems in trolleybus grids. J Clean Prod 2023;384:135623. https://doi.org/10.1016/J.JCLEPRO.2022.135623
[64] Welcome - KNMI data platform - KNMI data platform. 2024. https://dataplatform.knmi.nl/.
[65] Bezanson J, Edelman A, Karpinski S, Shah VB. Julia: a fresh approach to numerical computing. SIAM Rev 2017;59(1):65–98. https://doi.org/10.1137/141000671
[66] Lubin M, Dowson O, Garcia JD, Huchette J, Legat B, Vielma JP. JuMP 1.0: recent improvements to a modeling language for mathematical optimization, arXiv (May, 2022). http://arxiv.org/abs/2206.03866.
[67] Pulsipher JL, Zhang W, Hongisto TJ, Zavala VM. A unifying modeling abstraction for infinite-dimensional optimization. Computers Chem Eng 2022;156:107567. https://doi.org/10.1016/j.compchemeng.2021.107567
[68] Boyd S. Convex optimization. New York, NY, USA: Cambridge University Press; 2011. https://doi.org/10.1145/2020408.2020410. https://dl.acm.org/doi/10.1145/2020408.2020410.
[69] Prat E, Lusby RM, Morales JM, Pineda S, Pinson P. How long is long enough? finite-horizon approximation of energy storage scheduling problems, arXiv (Nov, 2024). http://arxiv.org/abs/2411.17463.
[70] Darivianakis G, Eichler A, Smith RS, Lygeros J. A Data-Driven stochastic optimization approach to the seasonal storage energy management. IEEE Control Syst Lett 2017;1(2):394–9. https://doi.org/10.1109/LCSYS.2017.2714426. http://ieeexplore.ieee.org/document/7945264/.
[71] Li Y, Vilathgamuwa DM, Quevedo DE, Lee CF, Zou C. Ensemble nonlinear model predictive control for residential solar battery energy management. IEEE Trans Control Syst Technol 2023;31(5):2188–200. https://doi.org/10.1109/TCST.2023.3291540. https://ieeexplore.ieee.org/document/10186024/.
[72] Konsman MJ, Wijbrandi WE, Huitema GB. Unlocking residential energy flexibility on a large scale through a newly standardized interface. In: 2020 IEEE power & Energy Society Innovative smart Grid Technologies Conference (ISGT). IEEE; 2020. p. 1–5. https://doi.org/10.1109/ISGT45199.2020.9087658. https://ieeexplore.ieee.org/document/9087658/.